Quantitative Phosphoproteomic Analysis Reveals Shared and Specific Targets of Arabidopsis Mitogen-Activated Protein Kinases (MAPKs) MPK3, MPK4, and MPK6

Naganand Rayapuram, Jean Bigeard, Hanna Alhoraibi, Ludovic L. Bonhomme, Anne-Marie Hesse, Joelle Vinh, Heribert Hirt, Delphine Pflieger

Quantitative Phosphoproteomic Analysis Reveals Shared and Specific Targets of *Arabidopsis* Mitogen-Activated Protein Kinases (MAPKs) MPK3, MPK4, and MPK6*[S]

Naganand Rayapuram‡‖‖, Jean Bigeard§¶‖‖, Hanna Alhoraibi‡‖‖, Ludovic Bonhomme‖, Anne-Marie Hesse**, Joëlle Vinh‡‡, Heribert Hirt‡¶¶, and Delphine Pflieger**§§

In Arabidopsis, mitogen-activated protein kinases MPK3, MPK4, and MPK6 constitute essential relays for a variety of functions including cell division, development and innate immunity. Although some substrates of MPK3, MPK4 and MPK6 have been identified, the picture is still far from complete. To identify substrates of these MAPKs likely involved in cell division, growth and development we compared the phosphoproteomes of wild-type and *mpk3*, *mpk4*, and *mpk6*. To study the function of these MAPKs in innate immunity, we analyzed their phosphoproteomes following microbe-associated molecular pattern (MAMP) treatment. Partially overlapping substrates were retrieved for all three MAPKs, showing target specificity to one, two or all three MAPKs in different biological processes. More precisely, our results illustrate the fact that the entity to be defined as a specific or a shared substrate for MAPKs is not a phosphoprotein but a particular (S/T)P phosphorylation site in a given protein. One hundred fifty-two peptides were identified to be differentially phosphorylated in response to MAMP treatment and/or when compared between genotypes and 70 of them could be classified as putative MAPK targets. Biochemical analysis of a number of putative MAPK substrates by phosphorylation and interaction assays confirmed the global phosphoproteome approach. Our study also expands the set of MAPK substrates to involve other protein kinases, including calcium-dependent (CDPK) and sugar nonfermenting (SnRK) protein kinases. ***Molecular & Cellular Proteomics 17: 10.1074/mcp.RA117.000135, 61–80, 2018.***

MAPK cascades are essential components of signal transduction in eukaryotes. These modules are composed of a MAPK kinase kinase (MAPKKK),[1] a MAPK kinase (MAPKK) and a MAPK, and transduce extracellular stimuli into multiple cellular responses via the phosphorylation of MAPK substrates. Phosphorylation can modify major properties of proteins, such as their enzyme activity, subcellular localization, as well as their stability and interaction with other proteins (1).

In Arabidopsis, MPK3, MPK4, and MPK6 have been implicated in the regulation of cell cycle, cytokinesis, plant development and innate immunity (2). The involvement of the MAPK module ANP2/ANP3 and MPK4 along with its target MAP65–1 is essential for microtubule organization and cytokinesis and *mpk4* plants are extremely dwarfed (3). MPK4 was localized to the cell plate in root tip cells and was shown to be required for cell plate formation (4). MPK3 and MPK6, together with the upstream MAPKKK YODA, were found to play a critical role in the formation, number and patterning of stomata. Although mutants lacking YODA accumulated many stomata, inducible RNAi double mutants of *mkk4*/*mkk5* and *mpk3*/*mpk6* exhibit clustered stomatal patterning indicating that the specification of stomata and pavement cells are disrupted (5). Recently, it was shown that the MKK7-MPK6 cascade plays a role in shoot branching by phosphorylation of its downstream target PIN1 whereas the MKK7-MPK3 cas-

From the ‡Center for Desert Agriculture, 4700 King Abdullah University of Science and Technology (KAUST), Thuwal, Saudi Arabia; §Institute of Plant Sciences Paris-Saclay IPS2, CNRS, INRA, Université Paris-Sud, Université Evry, Université Paris-Saclay, Bâtiment 630, 91405 Orsay, France; ¶Institute of Plant Sciences Paris-Saclay IPS2, Paris Diderot, Sorbonne Paris-Cité, Bâtiment 630, 91405 Orsay, France; ‖UMR INRA/UBP Génétique, Diversité et Écophysiologie des Céréales, Université de Clermont-Ferrand, 63039 Clermont-Ferrand, France; **CEA, BIG-BGE-EDyP, U1038 Inserm/CEA/UGA, 38000 Grenoble, France; ‡‡ESPCI Paris, PSL Research University, Spectrométrie de Masse Biologique et Protéomique (SMBP), CNRS USR 3149, 10 rue Vauquelin, F75231 Paris cedex05, France; §§CNRS, LAMBE UMR 8587, Université d'Evry Val d'Essonne, Evry, France

Received June 27, 2017, and in revised form, October 27, 2017
Published, MCP Papers in Press, November 22, 2017, DOI 10.1074/mcp.RA117.000135

Author contributions: N.R., J.B., H.A., H.H., and D.P. designed research; N.R., J.B., H.A., J.V., and D.P. performed research; N.R., J.B., H.A., L.B., and D.P. contributed new reagents/analytic tools; N.R., J.B., H.A., L.B., A.-M.H., J.V., H.H., and D.P. analyzed data; N.R., J.B., H.A., L.B., H.H., and D.P. wrote the paper.

[1] The abbreviations used are: MAPK, mitogen-activated protein kinase; MAMP, microbe-associated molecular pattern; MTI, MAMP-triggered immunity; XIC, extracted ion chromatogram; BiFC, bimolecular fluorescence complementation; ROS, reactive oxygen species; CDPK, calcium-dependent protein kinase; IMAC, immobilized-metal affinity chromatography.

cade regulates leaf development (6). MAPKs have also been implicated in the inducible defense system of plants, both on recognition of microbe-associated molecular patterns (MAMPs) leading to MAMP-triggered immunity (MTI) and during effector-triggered immunity (ETI) (7). MTI is induced by the sensing of MAMPs by plant pattern-recognition receptors (PRRs) (8). One such MAMP is the N terminus of bacterial flagellin, represented by the 22-amino acid-long peptide flg22 from *Pseudomonas aeruginosa* (9). In Arabidopsis, recognition of flg22 by the PRR flagellin-sensitive 2 (FLS2) together with its co-receptor BAK1 activates Ca^{2+} influx, production of reactive oxygen species (ROS) and phytohormones, as well as CDPKs and MAPKs (8). These defense responses also include stomatal closure to restrict pathogen entry (10, 11), callose deposition to reinforce the cell walls (12), and the production and secretion of antimicrobial molecules such as the phytoalexin camalexin and PR1 protein (13–16). Arabidopsis MPK3, MPK4, MPK6 and recently also MPK1, MPK11, and MPK13 are transiently activated in response to MAMP treatments (17–21). In response to flg22 sensing, at least two MAPK modules are activated: MKK4/MKK5-MPK3/MPK6 (17, 22) and MEKK1-MKK1/MKK2-MPK4 (20, 23). The MKK4/MKK5-MPK3/MPK6 module is thought to positively regulate immunity (24). The MEKK1-MKK1/MKK2-MPK4 module was originally considered to negatively regulate immunity (20, 23, 25–27), but subsequent work showed that this module is guarded by the R protein SUMM2, explaining the constitutive defense responses present in mutants of the MEKK1-MKK1/MKK2-MPK4 cascade (28–30). Recently, we performed a genome-wide transcriptome analysis of responses triggered by flg22 in wild-type (WT) and *mpk3*, *mpk4*, and *mpk6* plants, revealing both specific and cooperative functions of MPK3, MPK4, and MPK6 in immunity (31).

Targeted experiments and more systematic approaches have so far allowed the identification of several confirmed or putative substrates of these three immune MAPKs (32–34). However, these studies were done either *in vitro* or with inducible systems of upstream regulators which bear inherent problems of overexpression and specificity. Here, we quantitatively compared the cytoplasmic phosphoproteomes of WT and *mpk3*, *mpk4*, and *mpk6* mutant plants under ambient conditions and on MAMP stimulation. We identified 152 differentially phosphorylated peptides in response to flg22 treatment and/or when compared among genotypes. Seventy of these phosphopeptides could be classified as putative MAPK targets, which was further confirmed by biochemical analysis on seven proteins, with phosphosites that are specific to one or shared by several MAPKs. Overall, our work largely expands the repertoire of putative MAPK substrates, and confirms previous genetic and transcriptomic analysis (31) by providing the biochemical basis for the specific and partially overlapping roles of the three MAPKs in plant growth and defense.

EXPERIMENTAL PROCEDURES

Plant Material and Culture Conditions—For phosphoproteomic experiments, *Arabidopsis thaliana* ecotype Columbia-0 (Col-0) was used as wild-type (WT) plant. The mutants were *mpk3–1* (SALK_151594) (35), *mpk4–2* (SALK_056245) (4), and *mpk6–2* (SALK_073907) (35) which were all generated in Arabidopsis ecotype Col-0. Plants were grown, treated and harvested as described in (34). Three biological repeats were prepared for *mpk3*, *mpk4* and *mpk6* mutant plants and four repeats were obtained from WT plants, three of which had already been examined within our former study (34). Within each biological repeat, one sample was treated for 15 min with water and another sample for the same duration with 1 μM flg22 (final concentration). In the case of *mpk4* mutant, the *mpk4–2* mutation was segregating. $mpk4^{-/-}$ seedlings were thus first isolated based on their root phenotype (*i.e.* shortening and thickening of the primary root) (4). Selected seedlings were then transferred to liquid medium with the growth conditions mentioned previously (34) which allowed reverting the severely dwarf phenotype of *mpk4*.

Protein Isolation and Phosphopeptide Enrichment—Cytoplasmic protein fractions were obtained, proteins were precipitated and then proteolyzed with trypsin and phosphopeptides were enriched using the IMAC resin as described in (34).

Immunoblotting—About 80–100 mg of plant ground in a mortar with liquid nitrogen were resuspended in 200 μl of a buffer containing 50 mM Tris-HCl pH 7.5, 150 mM NaCl, 0.1% Nonidet P-40, 5 mM EGTA, 0.1 mM DTT (Sigma-Aldrich, Darmstadt, Germany), protease inhibitors (Complete mixture, Roche, and 1 mM PMSF, Sigma-Aldrich), and phosphatase inhibitors (1 mM NaF, 0.5 mM Na_3VO_4, 15 mM β-glycerophosphate, 15 mM 4-nitrophenyl phosphate, Sigma- Aldrich chemicals). The suspension was centrifuged at 20,000 g for 15 min at 4 °C, and the supernatant (150 μl) was collected. Protein quantification was carried out by Bradford method (B6916, Sigma-Aldrich), and the normalized protein amounts of all samples were denatured with SDS-sample buffer by boiling them at 95 °C for 10 min. Protein samples were resolved by SDS-PAGE at a constant amperage of 15 mA and transferred onto methanol-activated PVDF membranes (GE Healthcare, Chalfont St. Giles, UK) for 1 h at a constant voltage of 100 V. Blots were blocked with 5% BSA (A9647, Sigma-Aldrich) in 1× TBST for 1 h and then probed with Phospho-p44/42 MAPK (Erk1/2) (Thr202/Tyr204) (D13.14.4E) XP rabbit monoclonal antibody (#4370, Cell Signaling Technology, Danvers, MA), hereafter referred to as anti-pTpY antibody, at a dilution of 1:1,500 in 5% BSA in 1x TBST overnight at 4 °C. The membranes were washed three times with 1x TBST. Goat anti-rabbit antibodies (at a dilution of 1:15,000 in 5% BSA in 1x TBST) conjugated to horseradish peroxidase were used as secondary antibodies. The membranes were washed again three times with 1x TBST, and the antigen-antibody interaction was detected with enhanced chemiluminescence reagent (ECL Prime, GE Healthcare) using an imaging system (ChemiDoc MP System, Bio-Rad, Hercules, CA). Coomassie blue staining of blots was then carried out for protein visualization.

LC-MS/MS Analyses of Phosphopeptide Samples—LC-MS/MS analyses of IMAC-enriched phosphopeptide samples were performed exactly as detailed in (34). Briefly, a Dual Gradient Ultimate 3000 chromatographic system (Dionex, Sunnyvale, CA) was interfaced to an LTQ-Orbitrap XL ETD mass spectrometer (Thermo-Fisher Scientific, Waltham, MA). Phosphopeptide samples were separated on a C18 capillary column (Acclaim PepMap C18, 15 cm length x 75 μm I.D. x 3 μm particle size, 100 Å porosity, Dionex) with a gradient starting at 100% solvent A (water/ACN/formic acid, 95/5/0.1, v/v/v), ramping to 50% solvent B (water/ACN/formic acid, 20/80/0.1, v/v/v) over 60 min, then to 100% solvent B over 3 min (held 10 min), and finally decreasing to 100% solvent A in 3 min. The Orbitrap was operated in positive ionization mode, using the lock mass option

(reference ion at m/z 445.120025) to ensure more accurate mass measurements in FTMS mode. The Orbitrap cell recorded signals between *m/z* 400 and 1400 in profile mode with a resolution set to 30,000 in MS mode. When performing electron transfer dissociation (ETD) analysis, a charge-state dependent reaction time was used according to the formula CS-depRT × 2/z ms, with z being the precursor charge state. Supplemental activation was set to 20% in the Tune Page to increase ETD fragmentation efficiency. A total of five LC-MS/MS analyses alternating multistage activation (36) and ETD fragmentation spectra on the three precursor ions giving highest signals in MS were acquired on each phosphopeptide sample. After a first exploratory run targeting ionic species of charge states 2, 3, or 4, the following analyses used an iteratively updated exclusion list of the m/z values previously leading to peptide identifications. The successive use of MSA and ETD was meant to maximize the success rate of peptide identification, in terms of precise phosphosite assignment from the MS/MS spectra (34, 37). The acquired data were interpreted using Mascot, followed by our in-house developed tool FragMixer which allows merging the phosphopeptide identifications provided by paired MS/MS spectra and validating precise phosphosite positioning or maintaining ambiguity on phosphate group localization based on the Mascot-Delta score (MD-score) (38).

LC-MS/MS Analyses of Whole Cytoplasmic Protein Digests—To estimate the impact of flg22 treatment and/or genetic background on the relative abundance of whole proteins, we sought to identify them by nonmodified peptide sequences, by performing the analysis of total cytoplasmic extracts after tryptic digestion. Protein samples were reduced, alkylated and proteolyzed exactly as those prepared for phosphopeptide enrichment. A capillary liquid chromatography (Dual Gradient Ultimate 3000 chromatographic system (Dionex)) system coupled to a Q-Exactive instrument (Thermo-Fisher Scientific) was used to carry out LC-MS/MS analyses. Peptides were separated using a gradient starting at 100% solvent C (water/ACN/formic acid, 98/2/0.1, v/v/v), maintained for 5 min, then ramping from 3% to 46% solvent D (water/ACN/formic acid, 10/90/0.1, v/v/v) over 60 min, then to 90% solvent D over 10 min, flushing the column for 10 min at this buffer composition, and finally decreasing to 100% solvent C in 3 min to re-equilibrate the column for 20 min. The ten ions giving rise to the highest signals in MS were selected for MS/MS. Spectra were recorded in MS between *m/z* 400 and 1500 in profile mode; target resolution in MS was set to 70,000, the automatic gain control (AGC) was 10^6 and the maximum injection time was 250 ms. MS/MS spectra were acquired with a resolution set to 17,500, an AGC of 5×10^4, a maximum injection time of 120 ms, a normalized collision energy of 30% and an isolation window of 2 *m/z*.

MS Data Interpretation—RAW data files acquired on phosphopeptide samples on the LTQ-Orbitrap XL ETD instrument were processed using the software Proteome Discoverer 1.3 (Thermo Scientific) as interface. Two different workflows were created to handle MSA or ETD data separately. For ETD spectra interpretation, the workflow included a nonfragment filter node that removed a 4-Da window around the selected precursor ion, a 2-Da window around charge-reduced precursors and a 2-Da window around known neutral losses up to 120 Da in mass listed in (39). Database searches were performed with the Mascot server v2.2.07 while specifying the following parameters: database TAIR10 (release 2010/12/14, 35386 sequences); enzymatic specificity: tryptic with two allowed missed cleavages; fixed modification of cysteine residues (Methylthio(C)); possible phosphorylation of S, T, and Y residues; 5 ppm tolerance on precursor masses and 0.6 Da tolerance on fragment ions. Fragment types considered were those specified in the configuration "ESI-trap" in the MSA workflow, and "ETD-trap" in the ETD workflow. The possible oxidation of methionine residues was ignored, because we verified that its addition did not allow increasing the number of unique phosphopeptides identified at a fixed false discovery rate (FDR) (37). The data was then processed using FragMixer (37), an in-house developed computational tool that collates the information provided by the database search engine Mascot, from two different spectra with respect to amino acid sequence and location of phosphosite using two simple filtering rules relying on the peptide scores and Mascot Delta scores (MD-scores). It is publically available and can be downloaded from http://proteomics.fr/FragMixer. FragMixer was used to reach an estimated FDR of 1% for all analyses and a false localization rate (FLR) of phosphosites below 5%. We specified MD-score thresholds associated to a FLR below 5% according to (38).

Relative phosphopeptide abundance was obtained using the program MassChroQ (40) which integrates in all the compared runs the areas of the extracted ion chromatograms (XICs) for every phosphopeptide identified in at least one given run. The XIC areas reconstituted by MassChroQ were then further handled as described in the paragraph "Statistical evaluation of relative phosphopeptide quantification."

LC-MS/MS analyses of cytoplasmic samples with the Q-Exactive instrument were interpreted using MaxQuant version 1.4.1.2. Search parameters were as follows: database TAIR10; enzymatic specificity: tryptic with two allowed missed cleavages; possible oxidation of Met residues and acetylation of protein N terminus; 5 ppm tolerance on precursor masses and 20 ppm tolerance on fragment ions. FDR was set to 1% for both peptide-spectrum matches and proteins. For quantification purposes, the alignment time window was set to 5 min and the match among run time windows was set to 1 min. Proteins were validated with at least 2 identified peptides including at least one unique peptide. Quantification of protein abundance was estimated from the LFQ values (41) calculated by MaxQuant that ensure normalization of total protein amount among samples. Quantification was based on unique peptides only. Proteins quantified by less than three peptides were rejected. We also demanded that proteins be reproducibly quantified in at least six out of the eight factor combinations to evaluate by an ANOVA their possible abundance variation.

Experimental Design and Statistical Rationale—Our goal was thus to identify substrates of MPK3, MPK4 and MPK6 in both normal growth conditions and after challenge with a simulated pathogen attack. Three biological repeats of cytoplasmic protein extracts were prepared for *mpk3*, *mpk4*, and *mpk6* mutant plants and four repeats were obtained from WT plants. Within each biological repeat, one sample was treated for 15 min with water and another sample for the same duration with 1 μM flg22 (final concentration). Five LC-MS/MS injections were acquired on each phosphopeptide sample using an updated exclusion list. These iterative injections permitted improving quantification, by limiting the risks of missing values because of MassChroQ failing to realign properly the runs to be compared. The lists of phosphopeptides identified and quantified in these cytoplasmic proteins were finally processed as follows. In a first step, we performed WT/*mapk* pairwise comparisons of the phosphoproteomics data to identify phosphopeptides being completely nondetected in at least one condition. Phosphopeptide nondetection had to be systematic in all biological repeats. In parallel, phosphopeptide detection was deemed reproducible when an MS signal could be quantified in at least two out of the three biological repeats for mutant plants or in at least three out of the four repeats for WT plants. Nonreproducibly detected phosphopeptides were discarded from the data set.

To search for phosphopeptides exhibiting more subtle quantitative variations that depend on treatment, genetic background or both, we handled the data as follows. First, to compensate for the variable total peptide material injected on-column, each chromatographic peak (XIC) area was corrected by the median of the XICs measured in the considered run. Second, when a phosphopeptide was identified from ions of different charge states (*e.g.* z = 2, 3 and 4), each XIC asso-

ciated to a pep-z pair was considered individually. Indeed, even though we could verify that the amplitude/direction of variation (on flg22 treatment or change in genetic background) was comparable among ionic species of different charge states corresponding to the same identified phosphopeptide, the basal XIC areas were too different to allow considering the median of the areas associated to different charge states. Third, the median of the XIC areas detected for a given pep-z pair in the five iterative LC-MS/MS analyses was attributed to that pep-z pair. Fourth, we applied a filter to leave aside peptides for which XIC areas could not be measured reproducibly. We required that, for at least six out of the eight genotype x treatment combinations, a phosphopeptide be systematically detected (present) or nondetected (absent) in three biological repeats. A total of 804 phosphopeptide XICs out of 1608 quantified passed this filtering step. To identify phosphopeptides displaying significant abundance changes on flg22 treatment and to evidence their connections with changes that fall within *mapk* mutants, we designed a 2-way analysis of variance (ANOVA) using a linear model including the treatment and the genetic background as main grouping factors. The model used was: $Y_{ijk} = \mu + T_i + M_j + T \times M_{ij} + \varepsilon_{ijk;}$ where Y_{ijk} refers to individual pep-z pair abundance value, μ is the general mean, T_i is the treatment effect (mock *versus* flg22), M_j is the *mapk* mutation effect (WT, *mpk3*, *mpk4*, and *mpk6*), $T \times M_{ij}$ is the interaction effect of the main factors and ε_{ijk} is the residual. Phosphopeptides being flg22-dependent or genotype-dependent were extracted at a *p* value below 0.01.

Bioinformatic Analyses of Phosphorylated Proteins—Phosphorylated sequences identified with confident phosphosites were submitted to motif-x (http://motif-x.med.harvard.edu/motif-x.html) (42) to uncover over-represented phosphorylation patterns. Parameters set for the width, occurrences, significance, and background were 13, 20, 10^{-6}, and International Protein Index Arabidopsis proteome, respectively. These phosphorylated sequences were also submitted to STRING (43). We discarded nonconnected protein entries. The represented network was obtained at a ≪ medium confidence ≫ in data settings (min interaction score 0.4).

Putative MAPK docking sites were searched using the ELM program (http://elm.eu.org/) (44) with the UniProtKB identifier of the proteins of interest.

Gene Synthesis and Gateway™ Cloning—The coding sequences of AT3G29360 - UDP-GLUCOSE DEHYDROGENASE 2 (UGD2), AT5G43830 - Aluminum induced protein with YGL and LRDR motifs (AYL1), AT1G11360 - Adenine nucleotide alpha hydrolases-like superfamily protein or Universal Stress Protein A (USPA), AT1G50570 - Calcium-dependent lipid-binding (CaLB domain) family protein (CaLB), AT5G16880 - Target of Myb protein 1 (TOM1), AT4G00752 - PUX9, UBX domain-containing protein (PUX9) and AT3G49010 - BBC1, 60S ribosomal protein L13 (BBC1) were commercially synthesized from GenScript and cloned into the Gateway™ entry vector pENTR-D/Topo (Invitrogen, Carlsbad, CA). The genes were then shuttled by Gateway™ LR Clonase reaction (Invitrogen) into pDEST17 or pDEST-His-MBP for recombinant protein expression, into pBIFC1, pBIFC2, pBIFC3 and pBIFC4 (45) for bimolecular fluorescence complementation (BiFC) assay, and into pGWB5 (46) for subcellular localization.

Purification of Recombinant Proteins—His_6-tagged or His_6-MBP-tagged proteins and constitutively active MAPKs (kindly provided by J. Colcombet) (47) were expressed in *Escherichia coli* BL21-AI or Rosetta strains, respectively, and purified under native conditions using Ni-NTA agarose beads (Invitrogen Cat.No. R901–15) following manufacturer's instructions.

In Vitro Kinase Assays and Phosphosite Identification—Purified recombinant proteins and constitutively active MAPKs were mixed together in kinase reaction buffer (20 mM Tris-HCl pH 7.5, 10 mM $MgCl_2$, 5 mM EGTA, 1 mM DTT and 50 μM ATP) and incubated at ambient temperature for 30 min. SDS-sample buffer was added to stop the reaction followed by boiling at 95 °C for 10 min. Protein samples were resolved by SDS-PAGE. The gel was stained with SimplyBlue™ SafeStain (Novex cat. No. LC6065) and the band corresponding to the protein of interest was excised out, cut into small pieces of 0.5 mm^3 and destained with four successive washes of 15 min each with ACN and 100 mM NH_4HCO_3. Proteins were reduced with 10 mM Tris(2-carboxyethyl)phosphine (TCEP, C-4706 Sigma) in 100 mM NH_4HCO_3 at 37 °C for 1 h followed by alkylation with 20 mM S-Methyl methanethiosulfonate (MMTS, 64306 Sigma) at ambient temperature for 30 min. Proteins were then digested with trypsin (Porcine trypsin, Promega, Fitchburg, WI) at 37 °C overnight. The digestion was stopped by the addition of 1% formic acid and the peptides were recovered by incubating the gel pieces in ACN. The recovered peptide solution was desalted using C18 ZipTip® (Millipore, Burlington, MA, Cat. No. ZTC18S096) and analyzed by LC-MS/MS. Briefly, peptide samples were separated on a C18 column (Acclaim PepMap C18, 25 cm length × 75 μm I.D. × 3 μm particle size, 100 Å porosity, Dionex) connected to an LTQ-Orbitrap Velos or a Q-Exactive HF instrument. The LC gradient ramped from 5% solvent B (water/ACN/formic acid, 20/80/0.1, v/v/v) to 45% solvent B over 45 min, then to 90% solvent B for 10 min. The MS instrument acquired fragmentation spectra on the top 10 peptides using CID fragmentation in the LTQ-Orbitrap or HCD in the Q-Exactive instrument. RAW data files obtained were converted to MGF files using Proteome Discoverer interface (version 1.4). Database searches were performed with the Mascot server v2.4 specifying the following parameters: database TAIR10 (release 2010/12/14, 35386 sequences); enzymatic specificity: trypsin permitting two allowed missed cleavages; fixed modification of cysteine residues (Methylthio(C)); possible variable modifications of phosphorylation on S, T, and Y residues; 5 ppm tolerance on precursor masses and 0.5 Da tolerance on fragment ions. The results were filtered based on Mascot scores and MD-scores.

Bimolecular Fluorescence Complementation (BiFC)—To obtain the expression vectors, coding sequences of candidate genes and MAPKs (kindly provided by J. Colcombet) were cloned in fusion with the N- and C-terminal parts of YFP, either as N- or C-terminal fusions, under the control of the cauliflower mosaic virus 35S (CaMV-35S) promoter in the pBIFC1,2,3 and 4 vectors. Appropriate positive and negative controls were carried out for all combinations. Recombined vectors were individually transformed in *Agrobacterium tumefaciens* C58C1 strain by electroporation. *Agrobacterium* cultures from glycerol stocks were inoculated in 10 ml of LB medium with appropriate antibiotics and incubated for 24 h at 28 °C with agitation. Each culture was pelleted and resuspended in infiltration buffer (10 mM $MgCl_2$, 10 mM MES pH 5.7, 150 μM acetosyringone) to an OD_{600} of 1.5 and kept in the dark for 3 h. The P19 viral suppressor of gene silencing was coexpressed with each combination to prevent silencing of transiently expressed proteins (48). 500 μl of each bacterial culture were mixed before infiltration. For fluorescence complementation, all eight possible combinations between a candidate gene and a MAPK were agro-infiltrated into 3-week-old *Nicotiana benthamiana* leaves. After 3 days, an upright LSM 710 Zeiss confocal microscope with a 20X objective (Plan-Apochromat, NA 1.0) was used to visualize fluorescence. All images were acquired using Argon laser with 514-nm excitation.

GST Pull-down Assays—His_6-tagged or His_6-MBP-tagged candidate proteins and constitutively active GST-tagged MAPKs were expressed in *E. coli* BL21-AI or Rosetta strains. Ten μg of GST-MAPK protein lysates were incubated for 1 h at 4 °C with 50 μl of glutathione Sepharose 4B resin in 1 ml of binding buffer (25 mM Tris-HCl pH 7.4, 75 mM NaCl, 0.5 mM EDTA, 0.5 mM DTT and 0.01% Triton X-100) supplemented with 1% protease inhibitor mixture. The resin was then

washed three times with binding buffer and incubated for 4 h at 4 °C with 10 μg of candidate protein lysates in 1 ml binding buffer. The resin was then washed four times and bound proteins were eluted in SDS-sample buffer, denatured for 10 min at 95 °C, and subjected to SDS-PAGE followed by immunoblotting analysis, as described earlier, using anti-His antibody (Qiagen, Hilden, Germany, Penta-His Antibody Cat. No 34660). Blots were stained with Ponceau-S for visualization. *E. coli* protein lysates expressing GST alone were used as negative controls.

Subcellular Localization—Coding sequences of candidate genes were cloned in fusion with GFP at their C-terminal part under the control of the CaMV-35S promoter, in the pGWB5 vector. Recombined vectors were transformed in *A. tumefaciens* C58C1 strain which were subsequently infiltrated into *N. benthamiana* leaves, and GFP fluorescence was visualized after 3 days, essentially as described earlier for BiFC.

RESULTS

Overview of Phosphoproteomes of WT and mapk Mutants—To identify phosphoproteins that exhibit changes in phosphorylation levels in any of the *mpk3*, *mpk4* and *mpk6* mutants, we performed a phosphoproteomic analysis of at least three independent biological repeats of WT plants and of *mpk3*, *mpk4*, and *mpk6* mutants after mock or 15 min treatment with flg22 (Fig. 1-*A*). Phosphopeptides were enriched from cytoplasmic protein extracts using IMAC and identified by LC-MS/MS. 1,279 different phosphopeptides differing in amino acid sequence and/or number of phosphorylation sites were identified, that corresponded to 731 unique proteins (supplemental Table S1, Fig. 1*A*). Compared with the list of phosphopeptide sequences present in the database PhosPhAt (21,646 phosphopeptides), we identified 193 novel phosphopeptides (supplemental Table S1). When considering the sequences with precise localization of phosphorylation, the total of 1919 phosphosites were identified within 79.2% of singly, 16.9% of doubly and 3.9% of ≥ triply phosphorylated peptides (Fig. 1*B*). They were additionally distributed into 80.4% Ser, 16.0% Thr and 3.6% Tyr residues (Fig. 1*C*).

To extract phosphorylation motifs from the dataset, the phosphopeptides identified with precise phosphosites were submitted to motif-x (49) (Fig. 1*D*, supplemental Table S1). The combined low-stringency (S/T)*P and high-stringency Px(S/T)*P MAPK motifs accounted for the largest peptide population, followed by the casein kinase motif SxxS* and the SnRK/CDPK "simple motif 1" (K/R)xx(S/T)* (50), which fits to the involvement of CDPKs in flg22 and biotic stress signaling (51, 52). However, the motifs S*DxE, S*ExE, S*xDD, S*xxE, and S*xE correspond to unknown acidophilic kinases.

To identify the differentially phosphorylated peptides (supplemental Table S2) that depend on any one of the three MAPKs in the absence of MAMP challenge (Fig. 1*E*) or in response to MAMP treatment (Fig. 1*F*), we performed WT/*mapk* pairwise comparisons for peptides that are absent in any one condition (supplemental Table S3) as well as analyzed the entire dataset by a two-way ANOVA statistical test for relative changes in phosphorylation levels (supplemental Table S4). A total of 152 different phosphorylated sequences (corresponding to 138 proteins) were identified in this way, of which 70 harbored an (S/T)*P site. The differentially phosphorylated peptides were grouped into two categories: those that depend on the genetic background of the three MAPKs under nonimmunity and those that depend on flg22 (immunity-dependent).

Relative Abundance of (Phospho) Proteins in WT and mapk Mutants—Because several hundred genes are differentially expressed in *mpk3*, *mpk4* and *mpk6* mutants (31), it was important to distinguish between changes in phosphorylation stoichiometry and changes in protein amounts (53–55). We therefore performed LC-MS/MS analyses of the total peptide extracts (supplemental Table S5). Of the reproducibly quantified 1466 proteins, only two showed significant abundance variations on flg22 treatment ($p \leq 0.01$), 137 varied among genotypes ($p \leq 0.01$) and the abundance of 10 proteins depended on both genotype and flg22 treatment ($p \leq 0.05$) supplemental Table S5). More precisely, when comparing pairwise *mpki* mutant plants to WT plants, 10, 25 and 54 proteins appeared specifically differentially present in *mpk3, mpk4*, and *mpk6* mutants, respectively, compared with WT. In addition, 11 proteins were determined to be of affected abundance in all the mutants compared with WT plants. Interestingly, the genotype-dependent proteins were enriched in the GO terms "response to abiotic or biotic stress" (14.8%) and "response to stress" (16.1%) compared with the whole list of identified proteins (8.1% and 9.3%, respectively).

The phosphopeptides whose abundance changed among genotypes and/or by the treatment with flg22 (supplemental Tables S3 and S4) corresponded to 138 proteins, of which 75 were also detected by nonmodified sequences indicative of the whole protein amounts. Only six of these 75 proteins showed a change that depended on the genotype. We then compared the abundance of these six proteins and of their phosphopeptides among the eight conditions examined. For PGDH only, the protein abundance closely mirrors the variations in the F(stVGs)*DSDEYNPTLPKPR phosphopeptide levels: the lower amount of PGDH protein in *mpk6* is therefore the major factor for the apparent decrease in the $S^{67}TVGS^{71}D$ phosphorylation stoichiometry, which remains otherwise unchanged. Overall, we conclude that the large majority of phosphopeptide abundance changes observed are not because of variations in protein abundance but to differential phosphorylation.

Identification of MAPK Targets in Nonimmune Processes—All phosphopeptides quantified in the eight conditions are listed in supplemental Table S2. To identify phosphorylation events that depend on the respective MAPKs in nonimmune processes, we compared the phosphoproteomes of WT and *mpk3*, *mpk4*, and *mpk6* under unchallenged conditions. We obtained a total of 107 unique phosphopeptides corresponding to 102 proteins when comparing the *mapk* with the WT data (Table I and supplemental Table S6, established from

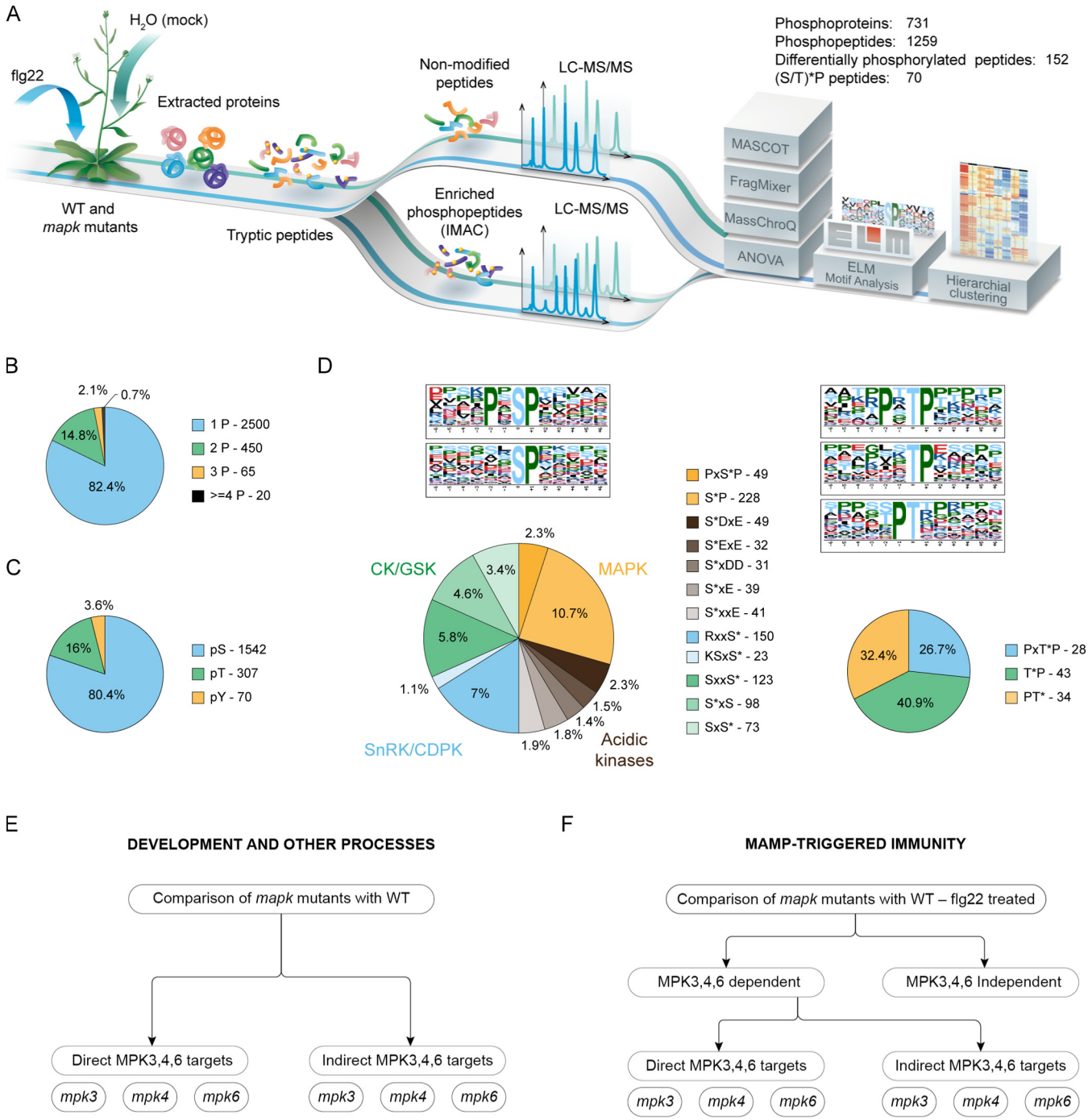

FIG. 1. ***A*, Schematic representation of the phosphoproteomics experimental workflow and data analysis for the identification of MAPK substrates.** Phosphopeptides were enriched using IMAC from WT plants and three *mapk* mutants treated with and without flg22 and analyzed by LC-MS/MS. Database searches were carried out using the program Mascot and phosphosite localization was ascertained using FragMixer. Relative quantification was carried out using MassChroQ, followed by statistical analysis of quantitative data to highlight sequences whose abundance was significantly modulated. The list of identified phosphopeptides was subjected to motif analysis using motif-x and ELM. The phosphopeptides identified for each of the samples were hierarchially clustered. *B*, Number of phosphorylation sites per peptide. *C*, Number of pS, pT and pY sites. *D*, Motifs enriched by Motif-X. *E*, Genotype-dependent phosphopeptides having a role in development and other processes grouped into direct and indirect MPK3, MPK4 and MPK6 targets. *F*, flg22-induced phosphopeptides having a role in MAMP-triggered immunity (MTI) grouped into MPK3-, MPK4- and MPK6-dependent and independent targets.

TABLE I

*This table lists all the (S/T)*P-containing phosphopeptides whose abundance was significantly diminished or increased in the considered mpki mutant compared to WT plants in mock condition (from supplemental Table S3 and Table S4 associated to supplemental Fig. S2). They thus constitute probable MAPK direct substrates. In bold characters are indicated phosphopeptides that were specifically non-detected in one mpki mutant; they thus constitute likely specific direct substrates of MPKi*

MAPK	Phosphopeptide	Protein_AGI	Protein_Description	mpki/WT
MPK3	HPR(t)*PPTNASLDYPSADSEHVSKR	AT1G15750	WSIP1, TPL Transducin family protein/WD-40 repeat family protein	0.00
	SKDNLYEQKPEEPVPVIPAA(s)*PTNDTSAAGSSFASR	AT5G46750	AGD9 ARF-GAP domain 9	0.00
	(t)*PSRLAGMFSGTQDK or TP(s)*RLAGMFSGTQDK	AT2G39900	GATA type zinc finger transcription factor family protein	2.09
	RVHAFPL(s)*PTSLLR	AT3G55270	MKP1, ATMKP1 mitogen-activated protein kinase phosphatase 1	infinity
MPK4	**SVETL(s)*PFQQK**	**AT1G07110**	**F2KP, ATF2KP, FKFBP fructose-2,6-bisphosphatase**	**0.00**
	HPR(t)*PPTNASLDYPSADSEHVSKR	AT1G15750	WSIP1, TPL Transducin family protein/WD-40 repeat family protein	0.00
	ITS(s)*PKQEIGTGEATEQEEGKEQK	**AT1G19870**	**iqd32 IQ-domain 32**	**0.00**
	VHNPVVESSIQPQR(s)*PR	**AT1G74690**	**IQD31 IQ-domain 31**	**0.00**
	ASGSPPVPVMH(s)*PPRPVTVK	**AT1G77180**	**SKIP chromatin protein family**	**0.00**
	SAIPDTRPR(t)*PIHESAATGR (3+)	**AT2G20960**	**pEARLI4 Arabidopsis phospholipase-like protein (PEARLI 4) family**	**0.00**
	SAIPDTRPR(t)*PIHESAATGR (4+)	**AT2G20960**	**pEARLI4 Arabidopsis phospholipase-like protein (PEARLI 4) family**	**0.00**
	KVV(t)*PLREMTPER	**AT2G25430**	**epsin N-terminal homology (ENTH) domain-containing protein**	**0.00**
	RRP(s)*L(s)*PPPPYR	**AT2G27100**	**S.E. C2H2 zinc-finger protein SERRATE (S.E.)**	**0.00**
	HVVDEPANEEKPSESSAAL(s)*PEK	**AT3G05900**	**neurofilament protein-related**	**0.00**
	FVYDK(s)*PEEVTGEEHGK	**AT3G16420/AT3G16430**	**PBP1, JAL30 PYK10-binding protein 1**	**0.00**
	YSVDM(s)*PVK	**AT3G26560**	**ATP-dependent RNA helicase, putative**	**0.00**
	R(s)*Y(s)*PGYEGAAAAAPDRDR	**AT3G55460**	**SCL30, At-SCL30 SC35-like splicing factor 30**	**0.00**
	SY(s)*PGYEGAAAAAPDRDR	**AT3G55460**	**SCL30, At-SCL30 SC35-like splicing factor 30**	**0.00**
	TTFVP(st)*PPALK TTFVP(s)*TPPALK	**AT3G63460**	**transducin family protein/WD-40 repeat family protein**	**0.00**
	NVEKVEEIR(s)*PQTINK	AT4G01290	unknown protein	0.00
	HYSEDVGEVQASQEKPV(s)*PK	**AT4G27430**	**CIP7 COP1-interacting protein 7**	**0.00**
	VVEEKPA(s)*PEPVKAEAEKPVEK	**AT5G35200**	**ENTH/ANTH/VHS superfamily protein**	**0.00**
	NTEEGEMVNNNV(s)*PMMHSR	AT5G45190	Cyclin family protein	0.00
	SKDNLYEQKPEEPVPVIPAA(s)*PTNDTSAAGSSFASR	AT5G46750	AGD9 ARF-GAP domain 9	0.00
	GMVSSGGPV(s)*PGPVYPGGRPGAGGLMPGMPGTR	AT5G57870	eIFiso4G1 MIF4G domain-containing protein/MA3 domain-containing protein	0.00
	SSWTSESYQLKPQSSFSGSHP(sGs)*PNAR	AT5G61960	AML1, ML1 MEI2-like protein 1	0.00
	FKVTSADL(s)*PK	**AT5G14720**	**Protein kinase superfamily protein**	**0.00**
	VLSL(s)*PSFRK	AT1G70290	ATTPS8, TPS8, ATTPSC trehalose-6-phosphatase synthase S8	0.44
	RY(s)*PPYYSPPR	AT3G55460	SCL30, At-SCL30 SC35-like splicing factor 30	0.57
	TVANSPEALQ(s)*PHSSESAFALK	AT5G43830	Aluminium induced protein with YGL and LRDR motifs	0.62
	LSYPT(s)*PALPKPR	AT5G03040	iqd2 IQ-domain 2	2.41
	(t)*PSRLAGMFSGTQDK or TP(s)*RLAGMFSGTQDK	AT2G39900	GATA type zinc finger transcription factor family protein	2.69
	AEALAALTSAFNSSPSSK(s)*PPRR	AT3G57410	VLN3, ATVLN3 villin 3	3.45
	DLSMNKFDWDHPLHLQPM(s)*PTTVK	AT3G29360	UDP-glucose 6-dehydrogenase family protein	infinity
	RVHAFPL(s)*PTSLLR	AT3G55270	MKP1, ATMKP1 mitogen-activated protein kinase phosphatase 1	infinity
MPK6	HPR(t)*PPTNASLDYPSADSEHVSKR	AT1G15750	WSIP1, TPL Transducin family protein/WD-40 repeat family protein	0.00
	(s)*PEHALFTKPVYDQTEQLPPAPWETQEPR	**AT1G21380**	**Target of Myb protein 1**	**0.00**
	SMTGEQIQAP(ss)*PRDGEDISITQGHPKPPALK	**AT1G30450**	**CCC1, ATCCC1, HAP5 cation-chloride co-transporter 1**	**0.00**
	KF(s)*EQNIGAPPSYEEAVSDSR(s)*PVYSER	**AT2G43160**	**ENTH/VHS family protein**	**0.00**
	NVEKVEEIR(s)*PQTINK	AT4G01290	unknown protein	0.00
	DAETVNQTSHPTEEEAQVTVSSNADVEDSHETV(s)*PR	**AT4G32330**	**TPX2 (targeting protein for Xklp2) protein family**	**0.00**
	TMEESETKPAD(t)*PDADKENTGEVQAEGAEDEDDEKEEK	**AT4G32720**	**AtLa1, La1 La protein 1**	**0.00**
	KR(sAPt)*(t)*PINQNAAAAFAAVSEEER	**AT4G37870**	**PCK1, PEPCK phosphoenolpyruvate carboxykinase 1**	**0.00**
	VVEEKPA(s)*PEPVKAEAEKPVEK	AT5G35200	ENTH/ANTH/VHS superfamily protein	0.00
	DIQGSDNAIPL(s)*PQWLLSKPGENK	**AT5G42950**	**GYF domain-containing protein**	**0.00**

MCP MOLECULAR & CELLULAR PROTEOMICS ASBMB

TABLE I—*continued*

MAPK	Phosphopeptide	Protein_AGI	Protein_Description	mpki/WT
	NTEEGEMVNNNV(s)*PMMHSR	AT5G45190	Cyclin family protein	0.00
	NTEEGEMVNNNV(s)*PMMHSR	AT5G45190	Cyclin family protein	0.00
	SKDNLYEQKPEEPVPVIPAA(s)*PTNDTSAAGSSFASR	AT5G46750	AGD9 ARF-GAP domain 9	0.00
	GMVSSGGPV(s)*PGPVYPGGRPGAGGLMPGMPGTR	AT5G57870	eIFiso4G1 MIF4G domain-containing protein/MA3 domain-containing protein	0.00
	SSWTSESYQLKPQSSFSGSHP(sGs)*PNAR	AT5G61960	AML1, ML1 MEI2-like protein 1	0.00
	AGDS(t)*PEELANATQVQGDYLPIVR	AT3G49010	ATBBC1, BBC1, RSU2 breast basic conserved	0.14
	FDWDHPLHLQPM(s)*PTTVK	AT3G29360/AT5G15490/ AT5G39320	UDP-glucose 6-dehydrogenase family protein	0.15
	YSLVLDPNLDAG(t)*PR	AT3G03570	Protein of unknown function (DUF3550/UPF0682)	0.16
	KTDGST(t)*PAYAHGQHHSIFSPATGAVSDSSLK	AT4G37870	PCK1, PEPCK phosphoenolpyruvate carboxykinase 1	0.23
	TDGST(tPAYAHGQHHSIFs)*PATGAVSDSSLK	AT4G37870	PCK1, PEPCK phosphoenolpyruvate carboxykinase 1	0.24
	SSVAEVTVPS(s)*PYKHEDPTEPDSREEESPALGAIR	AT3G43300	ATMIN7, BEN1 HOPM interactor 7	0.27
	NLSLNPTASAAPV(t)*PPKKDDKPEDILFK	AT1G21380	Target of Myb protein 1	0.31
	SKDSNVTPDDDVSGMR(s)*PSAFFK	AT3G13300	VCS Transducin/WD40 repeat-like superfamily protein	0.35
	YEEMNKPSAPLTSHEPAMIPVAEEPDD(s)*PIHGREESLVR	AT5G16880	Target of Myb protein 1	0.35
	FSSLSLLPSQT(s)*PK	AT3G55270	MKP1, ATMKP1 mitogen-activated protein kinase phosphatase 1	0.45
	FTDSALASAVF(s)*PTHK	AT2G41900	CCCH-type zinc finger protein with ARM repeat domain	0.45
	TVANSPEALQ(s)*PHSSESAFALK	AT5G43830	Aluminium induced protein with YGL and LRDR motifs	0.48
	AEALAALTSAFNSSPSSK(s)*PPR	AT3G57410	VLN3, ATVLN3 villin 3	0.48
	YVEEWVGPGSPMN(s)*PR	AT1G36310	S-adenosyl-L-methionine-dependent methyltransferases superfamily protein	0.51
	TLSYPTPPLNLQ(s)*PR	AT3G13300	VCS Transducin/WD40 repeat-like superfamily protein	0.51
	FTDSALASAVF(s)*PTHK	AT2G41900	CCCH-type zinc finger protein with ARM repeat domain	0.61

supplemental Tables S3, S4 and supplemental Fig. S2). A total of 51 peptides harbored one or two (S/T)*P motifs (Table I), 25 peptides contained an acidophilic motif (*e.g.* S*D or S*E) and 12 peptides the motif (K/R)xxS*, possibly corresponding to the activity of CDPKs and SnRK2s (supplemental Table S6). Among these sequences, phosphopeptides being absent in one *mapk* mutant while detected in the three other genotypes are clearly direct or indirect targets of the deleted MAPK. Whereas no phosphopeptides were specifically absent in *mpk3,* 34 and 14 phosphopeptides were undetectable in *mpk4* and *mpk6* mutants, respectively (Tables I and supplemental Table S6). Among these, 16 and 7 contained an (S/T)*P site (Table I), identifying them as putative direct substrates of MPK4 or MPK6, respectively, involved in processes such as various metabolic pathways, abiotic stress responses or plant development. Among *mapk* genotypes, 41 phosphopeptides from 38 proteins varied in abundance significantly (Tables I and supplemental Table S6, established from supplemental Table S4 and supplemental Fig. S2). Among these phosphopeptides, the majority showed reduced levels in a single *mapk*, indicating their preferential direct or indirect phosphorylation by that MAPK. Among these proteins, most were decreased in *mpk6*, with 16 bearing an (S/T)*P phosphosite (Table I) and 15 bearing other motifs, mostly acidic ones ((S)*(D/E)) (supplemental Table S6). The 16 phosphopeptides thus appeared to be direct whereas the 15 indirect MPK6 targets. Very few phosphopeptides exhibited decreased abundance in two mutants. For instance, TVANSPEALQ(s)*PHSSESAFAL from the Aluminum-induced protein with YGL and LRDR motifs AT5G43830 (later called AYL1) was less abundant in *mpk4* and *mpk6* mutants in untreated conditions (Table I), suggesting that this S*P site is targeted by both kinases.

Identification of flg22-induced Phosphorylation Targets and Contribution of MAPKs—To identify proteins related to MTI, we then looked for flg22-induced phosphorylated peptides in WT and *mpk3, mpk4*, and *mpk6* mutant plants and among these for probable MAPK targets. First, the absence of the dual phosphorylated activation loops TKSETDFM(t)*E(y)*VVTR in *mpk4* and VTSESDFM(t)*E(y)*VVTR in *mpk6* when compared with WT plants strengthened the robustness of our approach. The MS detection of these phosphopeptides on flg22 treatment correlated with the phosphorylation signals in immunoblotting experiments using an anti-pTpY antibody which recognizes the MAPKs in their activated form (supplemental Fig. S3).

A group of 19 phosphopeptides corresponding to 17 proteins were flg22-induced in a similar way in the four genotypes of WT and *mpk3, mpk4* and *mpk6* mutants (Table II, established from supplemental Tables S3 and S4). Overall, 18 of these 19 sequences contained an (S/T)*P site, which suggests that they are either targeted by MPK3, MPK4 or MPK6 in a redundant fashion or by yet other MAMP-induced MAPKs (21).

TABLE II

This table lists all the flg22-induced phosphopeptides (from supplemental Table S3 and Table S4 associated to supplemental Figure S2). The fold-changes of phosphorylation upon flg22 treatment are indicated for the four genotypes. "De novo" means that the phosphopeptides became de novo phosphorylated upon flg22 treatment. First, sequences becoming more phosphorylated on flg22 treatment are indicated. Then phosphopeptides being absent in one mutant in mock condition and showing different responses to MAMP application are listed

Phosphopeptide	Protein_AGI	Protein_Description	Fold-change WT	Fold-change mpk3	Fold-change mpk4	Fold-change mpk6
SPTWVTVQPS(s)*PRFPI(s)*TPTAGAQR	AT1G11360	Adenine nucleotide alpha hydrolases-like superfamily protein	de novo	de novo	de novo	de novo
KSPTWVTVQPS(s)*PRFPI(s)*TPTAGAQR	AT1G11360	Adenine nucleotide alpha hydrolases-like superfamily protein	de novo	de novo	de novo	de novo
HSFLDELK(s)*PNAR	AT3G20250	APUM5, PUM5 pumilio 5	de novo	de novo	de novo	de novo
SKDNLYEQKPEEPVPVIPAA(s)*PTNDTSAAGSSFASR	AT5G46750	AGD9 ARF-GAP domain 9	1.96	de novo	de novo	de novo
SVETL(s)*PFQQK	AT1G07110	F2KP, ATF2KP, FKFBP fructose-2,6-bisphosphatase	3.43	3.97	de novo	1.99
NLSLNPTASAAPV(t)*PPKKDDKPEDILFK	AT1G21380	Target of Myb protein 1	1.76	1.97	2.36	3.79
FTDSALASAVF(sPt)*HK (2+)	AT2G41900	CCCH-type zinc finger protein with ARM repeat domain	1.25	1.29	1.91	1.78
FTDSALASAVF(sPt)*HK (3+)	AT2G41900	CCCH-type zinc finger protein with ARM repeat domain	1.44	1.28	1.53	2.39
YSLVLDPNLDAG(t)*PR	AT3G03570	Protein of unknown function (DUF3550/UPF0682)	1.41	1.56	1.76	2.68
SKDSNVTPDDDVSGMR(s)*PSAFFK	AT3G13300	VCS Transducin/WD40 repeat-like superfamily protein	1.79	2.21	2.57	3.07
TLSYPTPPLNLQ(s)*PR	AT3G13300	VCS Transducin/WD40 repeat-like superfamily protein	2.12	1.65	1.82	2.11
AFAHPPEELN(s)*PASHFSGK	AT3G15450	Aluminium induced protein with YGL and LRDR motifs	4.82	4.51	4.87	4.24
SSVAEVTVP(ssPYKHEDPt)*EPDSREEESPALGAIR	AT3G43300	ATMIN7, BEN1 HOPM interactor 7	1.47	1.94	2.42	3.47
VSFAERP(s)*FK	AT3G54760	dentin sialophosphoprotein-related	2.17	1.65	1.89	1.32
YSLDNNPSSVL(s)*PR	AT4G00752	UBX domain-containing protein	1.99	1.91	1.75	1.50
(tPVPHsPPVVAs)**PIPPR	AT4G01810	Sec23/Sec24 protein transport family protein	17.75	de novo	de novo	de novo
VHEGAPDTEVLLA(s)*PR (2+)	AT4G31160	DCAF1 DDB1-CUL4 associated factor 1	1.53	2.20	2.59	1.62
VHEGAPDTEVLLA(s)*PR (3+)	AT4G31160	DCAF1 DDB1-CUL4 associated factor 1	2.49	2.13	2.37	2.14
ELLSELKSEEGDG(t)*PHSSASPFSR	AT5G41950	Tetratricopeptide repeat (TPR)-like superfamily protein	1.87	1.69	2.54	4.01
TVANSPEALQ(s)*PHSSESAFALK (2+)	AT5G43830	Aluminium induced protein with YGL and LRDR motifs	2.33	1.95	2.96	2.43
TVANSPEALQ(s)*PHSSESAFALK (3+)	AT5G43830	Aluminium induced protein with YGL and LRDR motifs	2.22	1.76	2.73	2.01
GMVSSGGPV(s)*PGPVYPGGRPGAGGLMPGMPGTR	AT5G57870	eIFiso4G1 MIF4G domain-containing protein/MA3 domain-containing protein	2.59	1.65	de novo	de novo
TTFVP(st)*PPALK	AT3G63460	transducin family protein/WD-40 repeat family protein	4.71	0.66	de novo	1.42
LS(t)*PKPLPSDLLHLK	AT1G06650	2-oxoglutarate (2OG) and Fe(II)-dependent oxygenase superfamily protein	de novo	de novo	de novo	NA
AEALAALTSAFNSSPS(s)*K(s)*PPR	AT3G57410	VLN3, ATVLN3 villin 3	de novo	NA	de novo	de novo
SMTGEQIQAP(ss)*PRDGEDISITQGHPKPPALK	AT1G30450	CCC1, ATCCC1, HAP5 cation-chloride co-transporter 1	1.19	1.28	1.45	de novo
QAAPVTGVPVAPTLDQRP(s)*R	AT1G32400	TOM2A tobamovirus multiplication 2A	1.24	0.86	0.00	de novo
FPSMEKPQFDHQN(s)*SVSSYGDLPELQRPETSPLDR	AT1G34220	Regulator of Vps4 activity in the MVB pathway protein	0.79	0.00	0.98	de novo
ASGSPPVPVMH(s)*PPRPVTVK	AT1G77180	SKIP	1.11	1.05	de novo	1.26
KF(s)*EQNIGAPPSYEEAVSDSR(s)*PVYSER	AT2G43160	ENTH/VHS family protein	0.59	0.99	2.00	de novo
ELDSS(sEAVsGNsDKVGADDLsDs)*EKEKPNLVGDGK	AT4G02510	TOC159, TOC86, PPI2, TOC160, ATTOC159	0.72	1.35	de novo	1.71
VEEEEEEDEIVE(s)*DVELEGDTVEPDNDPPQK	AT4G22670	AtHip1, HIP1, TPR11 HSP70-interacting protein 1	0.67	2.90	1.46	de novo
TDPIGLDNLSM(s)*DGESDPVYK	AT4G30890	UBP24 ubiquitin-specific protease 24	1.08	0.00	0.80	de novo
DAETVNQTSHPTEEEAQVTVSSNADVEDSHETV(s)*PR	AT4G32330	TPX2 (targeting protein for Xklp2) protein family	1.08	2.04	1.00	de novo
KR(s)*APT(t)*PINQNAAAAFAAVSEEER	AT4G37870	PCK1, PEPCK phosphoenolpyruvate carboxykinase 1	1.16	0.85	1.94	de novo
SAAND(tEMDDDs)*GNEKAGDDLSQDEIGVR	AT5G09390	CD2-binding protein-related	0.85	1.07	0.78	de novo
DIQGSDNAIPL(s)*PQWLLSKPGENK	AT5G42950	GYF domain-containing protein	0.71	2.70	2.21	de novo

Among phosphopeptides being absent in one *mapk* mutant in unchallenged conditions (Table I), some remained non-phosphorylated in that mutant on flg22 treatment, but others became phosphorylated. In the first category, the sequence LS(t)*PKPLPSDLLHLK from the 2-oxoglutarate (2OG) and Fe(II)-dependent oxygenase superfamily protein AT1G06650 became *de novo* phosphorylated in all studied genotypes on flg22 stimulation except in *mpk6* (Table II). This T*P site thus appears to be a specific direct target of MPK6 both under normal growth and MAMP signaling. In contrast, the second category of phosphopeptides was phosphorylated during MTI by another MAPK than the deleted one, maybe *via* a compensatory mechanism. One such example is SVETL(s)*PFQQK from F2KP, which is absent in *mpk4* mutant in mock condition, but is well detected on flg22 stimulation (Table II). Ten phosphopeptides of Table II were not detected in the *mpk6* mutant under mock conditions and showed no increase in phosphorylation levels in WT plants on flg22 treatment. However, these peptides became modified in flg22-stimulated *mpk6* plants. The latter sites are therefore targeted by other immune MAPKs when the plant needs to counteract a pathogen attack. Altogether, these observations highlight the interconnectivity of the MAPK cascades that contribute to MAMP signaling robustness.

The interaction of MAPKs with their substrates usually requires the presence of a MAPK docking site (D-site) (56). We thus searched for the possible presence of D-sites in the sequence of the proteins harboring (S/T)*P-modified peptides using the ELM program supplemental Table S3 and supplemental Table S4). The 67 phosphopeptides modulated in their abundance among genotypes and/or on flg22 stimulation corresponded to 62 unique proteins, 8 of which harbored one and 44 multiple MAPK D-sites.

Phosphopeptide Cluster Analyses Reveal Major Differences in MAPK Targets—To obtain a global view on the different *mapk* mutants, a cluster analysis was performed on the phosphopeptides exhibiting significant abundance variations between mutant and WT plants. As shown in supplemental Fig. S4, the biggest differences in the phosphoproteomes are found between *mpk6* and the other mutants and WT plants. Interestingly, most phosphopeptides are less abundant in *mpk6*, irrespective of whether these are phosphorylated on (S/T)*P or other motifs. Moreover, the phosphoproteome of *mpk3* is more closely related to that of *mpk4* than to *mpk6*, confirming our previous transcriptomic studies (31).

The global heat map of the nontreated and flg22-treated samples together (Fig. 2) clearly shows that a lack of any of the MAPKs strongly impacts the ability of the plant to respond properly to the flg22 stimulus. Finally, compared with WT, *mpk3* and *mpk4* mutants also show a partially overlapping pattern on flg22 treatment.

We obtained the phosphoproteome of each *mapk* mutant by collecting all phosphopeptides being significantly up- or down-regulated in that mutant when compared with WT plants. We then grouped the corresponding phosphoproteins into a protein interaction network using the program STRING (43) (Fig. 3). Networks could be retrieved for all three MAPKs (Figs. 3*A*–3*C*), with MPK4 and MPK6 giving the most extensive signaling networks.

Interaction Network of the MPK4 Phosphoproteome—MPK4 has a prominent role in cytoskeleton organization and cytokinesis. The MPK4 network is clearly linked to several microtubule-associated proteins (MAPs). Besides finding MAP65, we also identified VHNPVVESSIQPQR(s^{356})*PR and ITS(s^{680})*PKQEIGTGEATEQEEGKEQK as being absent in *mpk4,* indicating that MPK4 phosphorylates IQD31 and IQD32, respectively. Both proteins were reported to be MAPs (57) and several members of the IQD family play roles in plant development and basal defense response (58). MPK6 also seems to be implicated in phosphorylating proteins involved in the cytoskeleton. AEALAALTSAFNSSPSSK(s^{814})*PPR of VILLIN3, which participates in actin filament bundling, was affected in *mpk*6. In addition, a peptide containing S^{415}P of TPX2/WDL5, a MAP involved in the organization of the spindle apparatus (59), is absent only in *mpk6* in unchallenged conditions.

An interesting link also exists between MPK4 and the two CDPKs CPK5 and CPK6, which are important regulators of innate immunity and ROS production (51, 60). However, as the phosphopeptide sequences do not correspond to MAPK motifs but nonetheless depend on a functional MPK4, both proteins are indirect targets of MPK4.

Splicing of mRNA is an important process in all eukaryotes, and is also linked to stress responses in plants (61). Among the splicing factors, SCL30 has previously been identified by us to be phosphorylated *in vitro* by MPK3, MPK4, and MPK6 (62). Interestingly, SY(s^{206})*PGYEGAAAAAPDRDR, R(s)*Y(s^{206})*PGYEGAAAAAPDRDR and RY(s^{5})*PPYYSPPR from SCL30 were absent or reduced in *mpk4* (Fig. 4*A*). In the MPK4 network, SCL30 is connected to SKIP and the RNA helicase DHX8/PRP22 (AT3G26560) and phosphopeptides corresponding to SKIP and DHX8/PRP22 are missing in *mpk4,* suggesting that SCL30, SKIP, and DHX8/PRP22 are all *in vivo* substrates of MPK4.

Interaction network of the MPK6 phosphoproteome—As shown in Fig. 3*B*, MPK6 is linked to the dual specificity phosphatase MKP1 which regulates MAPK activation levels and is an important regulator of biotic and abiotic stress responses (63, 64). Interestingly, T^{64}, T^{109}, and S^{558} of MKP1 were shown to be phosphorylated by MPK6 *in vitro* (65) and MKP1 was suggested to be a substrate of MPK3, as MKP1 can still be phosphorylated in *mpk6* mutant plants (66). Because VHAFPL(s^{295})*PTSLLR and RVHAFPL(s^{295})*PTSLLR are both absent in *mpk3* treated by flg22, MKP1 is an *in vivo* target of MPK3 at S^{295}. In addition, FSSLSLLPSQT(s^{558})*PK from MKP1 is significantly less abundant in *mpk6* (Fig. 4*B* and supplemental Table S4), indicating that MPK6 phosphorylates MKP1 at S^{558}.

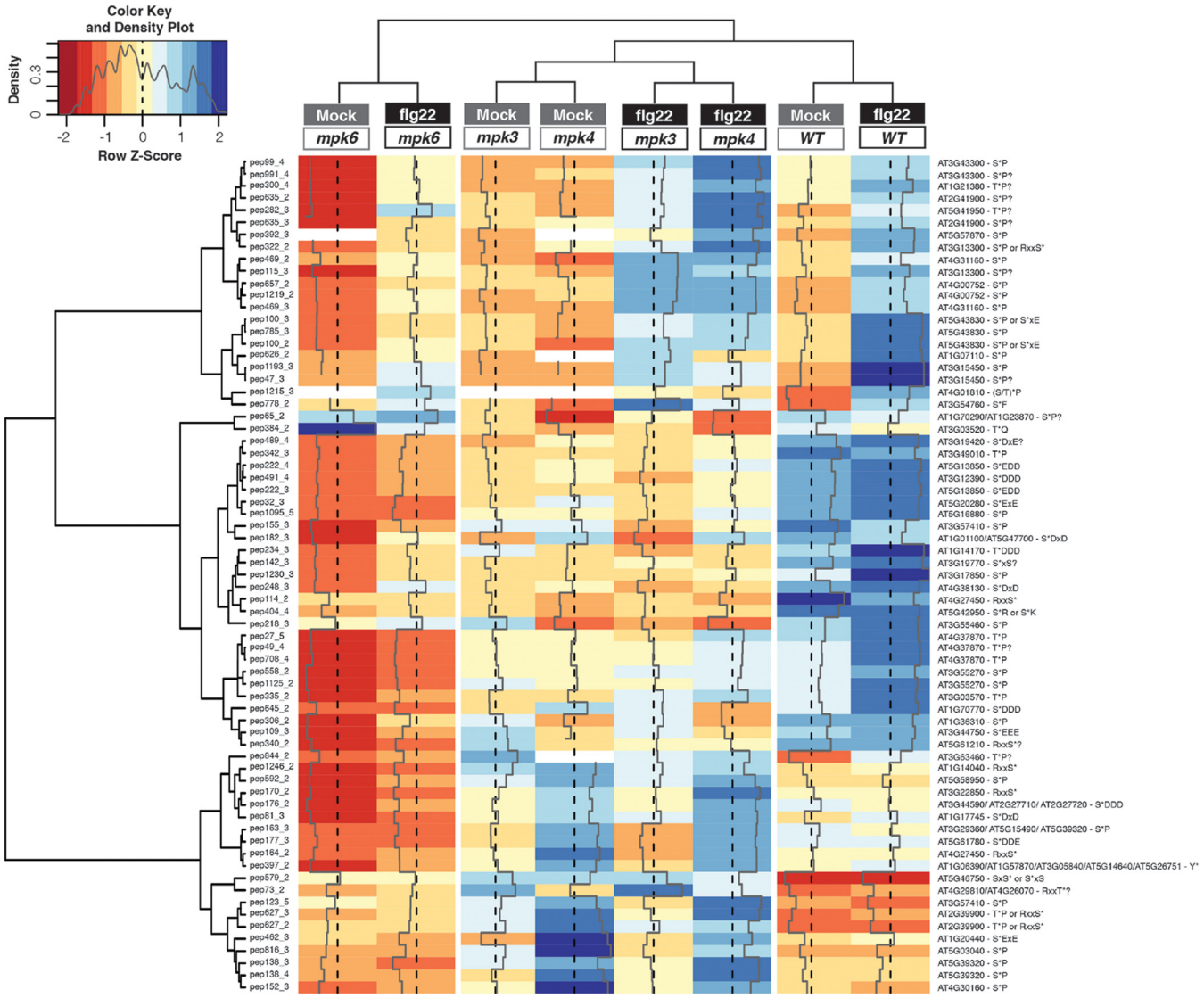

FIG. 2. **Heatmap showing the relative abundances among the eight studied conditions of phosphopeptides significantly affected by the genotype and/or the flg22 treatment.**

From the STRING-based analysis of the MPK6 phosphoproteome, a major network emerges linking MPK6 to two histone deacetylases, which are important in gene regulation. Because the corresponding HD1 and HD2A/HDA3 sequences [WDPD(s)*DMDVDDDRKPIPSR] and [TPNIEPQGY(s)*EEEEEEEEVPAGNAAK] are not MAPK motifs, these data indicate MPK6 as an upstream regulator of an HD1 and HD2A kinase. A most prominent hub of 10 proteins comprises exclusively ribosomal (BBC1, AT2G27710, AT1G01100/AT5G47700, AT2G27710/AT2G27720/AT3G44590, AT3G09200, AT3G11250; we separated by a slash the proteins that shared a phosphopeptide) or ribosome-associated proteins (NACA3 and AT3G12390). The phosphopeptide sequences of the 10 proteins do not correspond to MAPK motifs and hence are indirect targets of MPK6. These results suggest that MPK6 might play an important role in translational control.

On pathogen challenge, plants also modify their metabolism and MPK6 appears to be targeting several key metabolic enzymes, including key enzymes in carbon metabolism such as 3-phospho glycerate dehydrogenase (PGDH), sucrose phosphate synthase 1F (SPS1F) or phosphoenolpyruvate carboxykinase (PEPCK). T^{122} phosphorylation of PEPCK by MPK6 on flg22 challenge exemplifies its regulation (Fig. 4*C* and supplemental Table S3). Carbon metabolism and cell wall synthesis also seem to be targeted by MPK6, as shown by the three UDP-glucose dehydrogenases UGD2, 3, and 4.

In addition, three probable direct MPK6 targets which show up-regulation of their phosphosites on flg22 treatment were Varicose (VCS) and the unknown function proteins AT5G43830 and AT3G03570 (supplemental Table S4), thereby constituting additional possible MAPK substrates with a role in defense response.

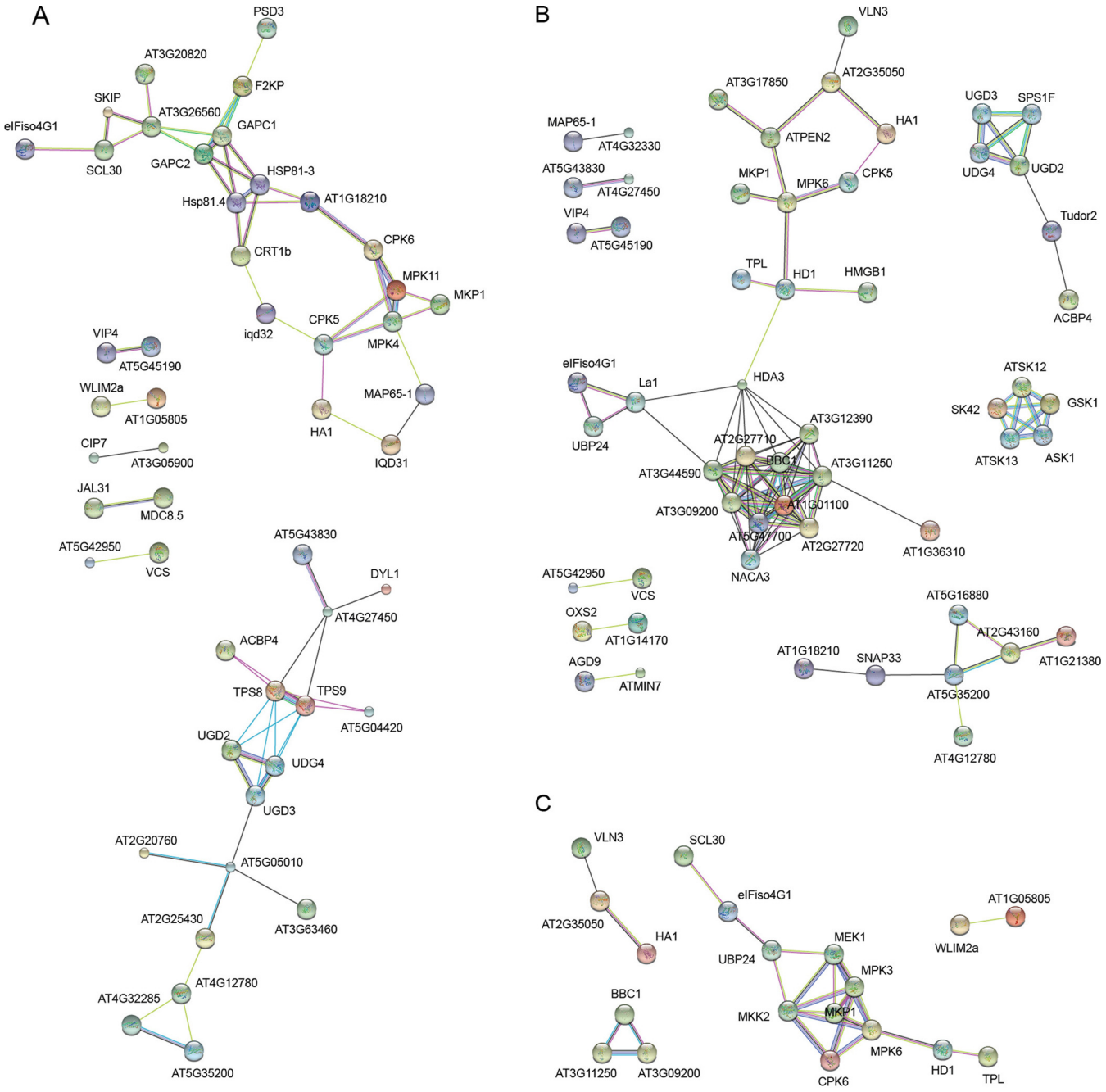

FIG. 3. **Protein interaction networks.** All the targets obtained for each of the MAPKs were pooled and used to generate a network using STRING (version 10.0). *A*, Network of targets of MPK4. *B*, Network of targets of MPK6. (C) Network of targets of MPK3.

Interaction Network of the MPK3 Phosphoproteome—The MPK3 phosphoproteome was the smallest of all three MAPKs (Fig. 3*C*). Nonetheless, several targets could be linked to MPK3. Most prominently, MPK3 was linked to several substrates that also appeared in other networks, such as MKP1, which was found in the MPK6 network. Similarly, CPK6 was shared with MPK4, and three of the 60S ribosomal proteins were shared with MPK6. However, two interesting MPK3-specific targets could also be identified: one is the plasma membrane H+ ATPase AHA1, which is of major importance for both abiotic and biotic stress conditions (67, 68) and the other is the deubiquitinase UBP24, which was shown to be an important regulator of ABA signaling (69). However, in both cases, MPK3 functions as an indirect regulator, as the respective phosphosites do not match the MAPK signature.

Interaction of Immune MAPKs with Their Putative Substrates—The assessment of the quantitative phosphoproteomic data suggested complex kinase-substrate relation-

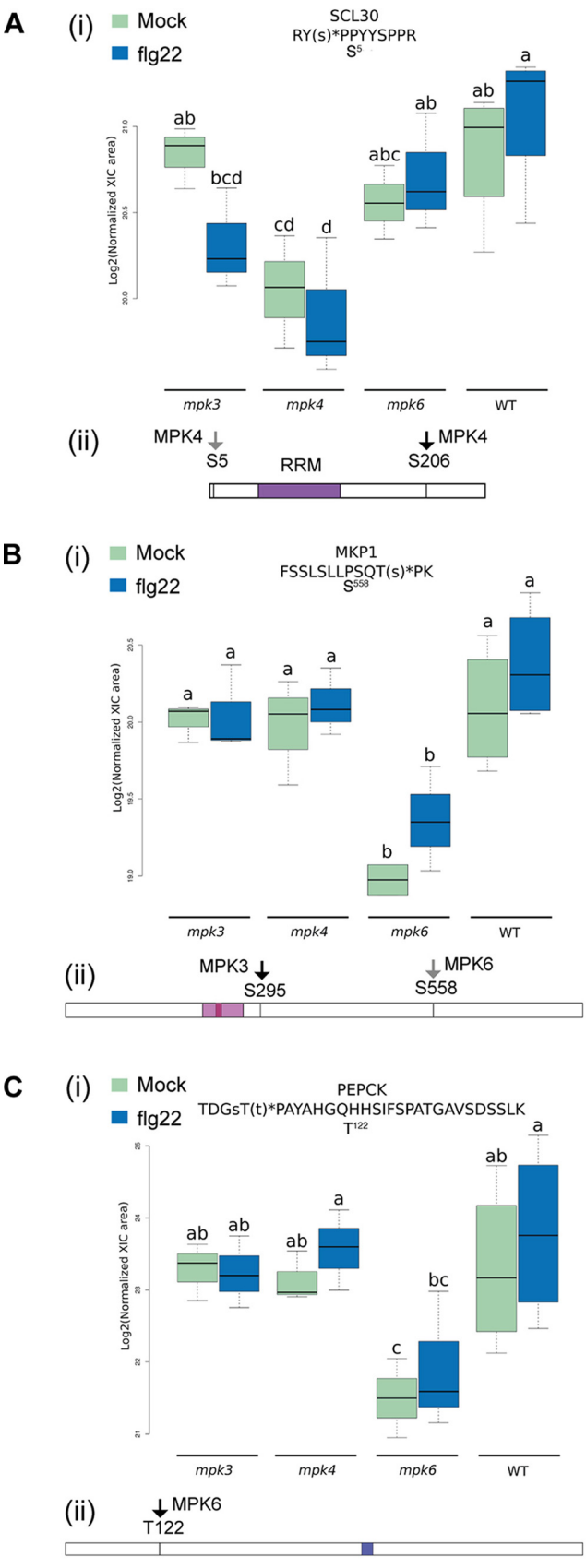

ships among MPK3, MPK4, and MPK6 and several tens of proteins as substrates. To test our conclusions, we selected seven proteins for further assays. These proteins were detected by (S/T)*P-containing phosphopeptides that belonged to the different categories: absent in at least one *mapk* mutant (Calcium-dependent lipid-binding family protein (CaLB) and Adenine nucleotide alpha hydrolases-like superfamily protein, also called Universal Stress Protein A (USPA)); induced by flg22 (UBX domain-containing protein (PUX9)); *mapk* genotype-dependent (Target of Myb protein 1 (TOM1); 60S ribosomal protein L13 (BBC1) and UDP-glucose dehydrogenase 2 (UGD2)); and finally, both flg22-induced and *mapk* genotype-dependent (Aluminum-induced protein with YGL and LRDR motifs (AYL1)).

The interaction among the three MAPKs and their putative targets was first tested *in vivo* by bimolecular fluorescence complementation (BiFC) assays in *N. benthamiana* (Fig. 5*A*). The interaction between AtMAP3K17 and AtMKK3 was used as a positive control of interaction in the cytosolic compartment as shown by Danquah *et al.* (70). The interaction of the candidate proteins with AtMAP3K17 was used as negative control. All the positive and negative controls are shown in supplemental Fig. S5. CaLB interacted with MPK3, MPK4, and MPK6 exclusively in the cytoplasm. The interaction of USPA and TOM1 with MPK3 and MPK4 was detected in the cytoplasm whereas their interaction with MPK6 was detected both in the cytoplasm and nucleus. The interaction of PUX9 with MPK3 was detected in the cytoplasm whereas the interaction with MPK4 and MPK6 was detected in both the cytoplasm and the nucleus. AYL1 interacted with MPK3 and MPK6, but not MPK4, in both the cytoplasm and the nucleus. UGD2 and BBC1 did not interact in these assays with any of the three MAPKs tested.

The interaction among the three MAPKs and their putative targets was also tested *in vitro* by GST pull-down assays (Fig. 5*B*). The interaction of the candidate proteins with GST alone was used as negative control, as well as the interaction of the three GST-MAPKs with His-MBP alone (Fig. 5*C*). TOM1 and UGD2 interacted with all the three MAPKs. USPA interacted specifically with MPK6. PUX9 and BBC1 did not interact with any of the three MAPKs. The strong interaction of CaLB and

FIG. 4. **Boxplots showing the relative abundance of a few phosphopeptides that exhibit a genotype-dependence.** *A*, (1) RY(s^{5})*PPYYSPPR (pep218) from SCL30; (2) Schematic representation showing the RNA Recognition motif (RRM) in purple and the phosphorylation sites. *B*, (1) FSSLSLLPSQT(s^{558})*PK (pep558) from MKP1; (2) Schematic representation showing the dual specificity phosphatase catalytic domain in pink, the protein-tyrosine phosphatase active site in dark pink and the phosphorylation sites. *C*, (1) (tDGsTt^{122})*PAYAHGQHHSIFSPATGAVSDSSLK (pep49) from PEPCK; (2) Schematic representation showing the phosphoenolypyruvate carboxykinase domain in blue and the phosphorylation sites. Specific phosphorylation sites are indicated with black arrows and preferential phosphorylation sites are indicated with gray arrows.

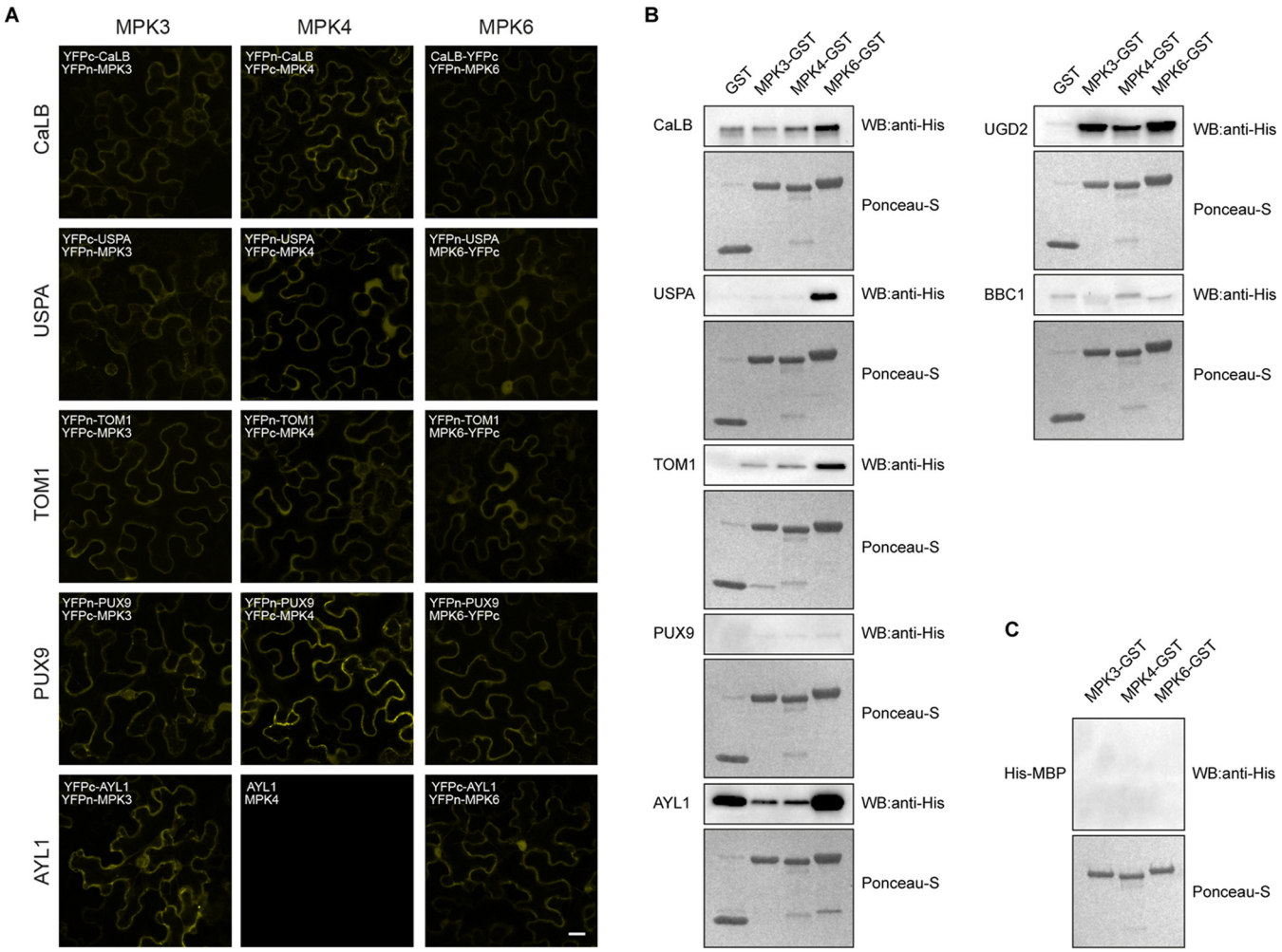

FIG. 5. ***A*, BiFC analysis of the seven tested MAPK candidate substrates with MPK3, MPK4 and MPK6 in *N. benthamiana* leaf epidermal cells.** YFP fluorescence was observed by laser scanning confocal microscopy. Scale bar = 20 μm. *B*, Glutathione S-transferase (GST) pull-down assays were performed by incubating bacterial lysates of GST (Lane1), MPK3-GST (Lane2), MPK4-GST (Lane3) and MPK6-GST (Lane4) with GST beads followed by incubation with bacterial lysates candidate proteins tagged with His tag or His-MBP tag. The pull-downs were probed with anti-His antibody (WB: anti-His) and the proteins were stained with Ponceau-S. *C*, A negative control for binding of His-MBP with the three MAPKs.

AYL1 with GST alone did not allow drawing relevant conclusions as to their interaction with the three MAPKs.

Overall, the direct physical interaction among six candidate proteins and the MAPKs was confirmed in at least one of the interaction assays.

Validation of Novel In Vivo Phosphorylation Sites of MAPK Substrates—The selected candidates were all phosphorylated *in vivo* on one or more (S/T)*P sites suggesting that they were potential substrates of MAPKs. To test the capacity of the MAPKs to phosphorylate these proteins at the given *in vivo* sites, the seven proteins were produced as recombinant proteins and tested by *in vitro* kinase assays (supplemental Table S7). TOM1 and BBC1 were phosphorylated by both MPK4 and MPK6; UGD2, AYL1, USPA, and PUX9 were phosphorylated by all three MAPKs. Except for CaLB, which was not phosphorylated by any of the three MAPKs, the *in vivo* phosphosites were phosphorylated by the respective MAPKs *in vitro*. In some cases, additional (S/T)*P sites were phosphorylated by the three immune MAPKs (supplemental Table S7). Overall, these results suggest that six out of the seven tested proteins represent true MAPK substrates.

Subcellular Localization of the MAPK Substrates—To further characterize the seven selected proteins, we examined the subcellular localization of GFP-tagged proteins expressed in *N. benthamiana* leaf epidermal cells by confocal microscopy (Fig. 6). Five of the candidate proteins, namely UGD2, USPA, TOM1, CaLB, and PUX9 were localized exclusively to the cytoplasm whereas AYL1 localized to both the cytoplasm and nucleus. BBC1, however, was localized exclusively to the nucleus. These subcellular localization data are overall in good agreement with the BiFC results and with the fact that these proteins were identified from a cytoplasmic fraction.

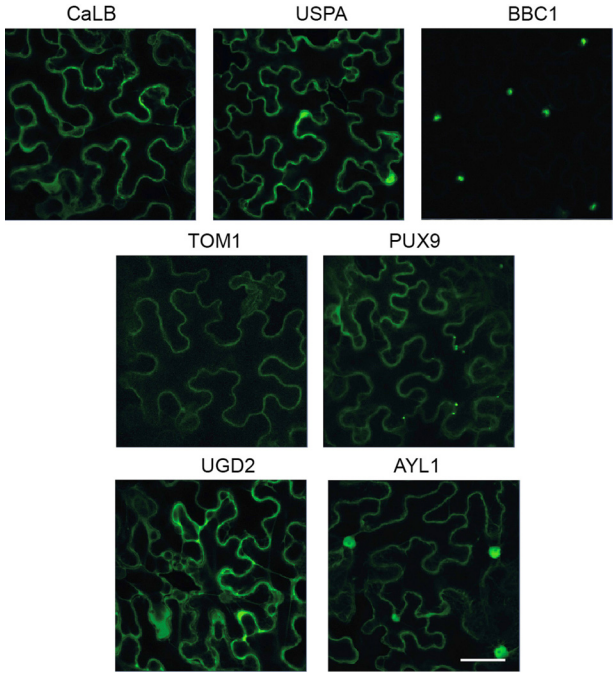

FIG. 6. **Subcellular localization of the seven transiently expressed MAPK candidate substrates fused to GFP driven by 35S promoter in *N. benthamiana* cells.** The tagged proteins were expressed in 4-week-old tobacco plants and the localization was visualized between 48 and 72 h after infiltration by laser scanning confocal microscopy. Scale bar = 50 μm.

DISCUSSION

Expansion of the MAPK Substrate Repertoire—Given the critical roles of MPK3, MPK4, and MPK6 in several processes, including development and in responses to environmental stresses, the identification of their substrates is of great interest. Here, we used a phosphoproteomic approach on WT plants and the three *mapk* mutants in the absence or on stimulation by the MAMP flg22 to identify putative *in vivo* substrates of MPK3, MPK4 and MPK6. According to our phosphoproteomic analyses, we identified 70 peptides as putative targets of one or several of the three MAPKs. Previously, Hoehenwarter *et al.* published a phosphoproteomic study on *A. thaliana* seedlings expressing tobacco NtMEK2^{DD} (32) to trigger the activation of MPK3 and MPK6. Among 35 putative MPK3/6 substrates, nine are found in our data set and seven harbor the same phosphosites (Table S8). Likewise, Lassowskat *et al.* reported a phosphoproteomic study on adult *A. thaliana* plants expressing the constitutively active PcMKK5^{DD} which activates MPK3 and MPK6 (33). The authors identified 538 probable phosphoproteins with altered abundance downstream of MPK3/6 activation, of which 30 are found in our dataset (Table S8). Common putative MAPK substrates were thus identified in these studies, although plant age, growth conditions and the technical approaches differed. Besides, we identified AT2G20760 (clathrin light chain) which was shown to be phosphorylated by MPK3 and MPK4 on protein microarrays (71), and AT1G11360 (adenine nucleotide alpha hydrolases-like superfamily protein) and AT1G30450 (CCC1) which were predicted to be MPK3 or MPK6 substrates based on the experimentally determined preferential phosphomotif of these kinases (72). However, no overlap exists among our list of putative MAPK substrates and the list of candidates obtained using protein microarrays incubated with MPK3 and MPK6 (73). Finally, one can note that we did not identify known MAPK substrates of lower abundance, such as WRKY transcription factors. Several reasons can account for this absence: we characterized every phosphopeptide using two fragmentation modes (CID and ETD), which reduced the total number of fragmented peptides by a factor of two, but increased the reliability of phosphosite identification; we analyzed a cytoplasmic protein fraction, which is of high complexity and is not expected to be the subcellular compartment best suited to detect transcription factors. Overall, our *in vivo* phosphoproteome results confirm the identification of several previously proposed MAPK targets and largely expand the repertoire of MAPK substrates.

MAPKs May Target Several Proteins of the Same Complex/Pathway—The protein interaction network analysis of phosphoproteins exhibiting modified phosphorylation levels highlighted that proteins belonging to the same complex or pathway may be collectively targeted by immune MAPKs as direct substrates and/or more indirectly by MAPKs acting as upstream regulators of the responsible kinases. We identified a number of proteins involved in translational control for both MPK3 and MPK6 and several cytoskeleton regulatory proteins for MPK4. Interestingly, putative substrates of the human ERK1/2 MAPKs identified by phosphoproteomics also appeared to group in protein complexes or functional pathways (74), which suggests the probable broad conservation of this feature among eukaryotes.

Specific and Shared MAPK Substrates—Our previous genetic and transcriptomic analysis indicated that MPK3, MPK4 and MPK6 had specific targets but also closely collaborate as kinase pairs or even as kinase triads to execute their functions (31). For example, approximately half of the genes that were differentially expressed in *mpk3* displayed a similar regulation in *mpk4*. Moreover, we observed that a knock out in *mpk3* or *mpk6* affects the activation of the other two kinases in the triad. Unfortunately, the basis for the interactive functioning of the three MAPKs could not be revealed from transcriptome data alone and further studies were necessary to unravel the underlying mechanisms. Principally, the MPK3, MPK4 and MPK6 phosphoproteomes largely confirm the previous observations, showing a highly complex pattern of phosphorylation events for some targets. Some phosphopeptides are exclusively absent in a single *mapk* mutant, indicating their specific direct or indirect modification by that MAPK. Others show a diminished abundance in one *mapk* mutant, indicating their favored but not exclusive phosphorylation by that MAPK.

Finally, a few proteins, such as AYL1, clearly appeared in the phosphoproteomics screen as shared targets of two MAPKs.

Regarding the question as to how different *mapk* mutants might affect the other MAPK pathways, it was hypothesized that phosphatases might play an important role. In fact, our data revealed that the dual-specificity phosphatase MKP1, which can regulate the activity of MPK3, MPK4 and MPK6 *in planta*, is targeted by MPK3 and MPK6. Interestingly, the two MAPKs target different sites in MKP1, as MPK3 phosphorylates S^{295} and MPK6 S^{558} (Fig. 4*B*). At present the biological function of these two sites is not clear, but certainly strengthens the idea that MKP1 could be a central regulator of the MAPK activation profiles. Another interesting factor of our phosphoproteome analysis was the identification of the deubiquitinase UBP24 as MPK3-specific target. UBP24 is an upstream regulator of ABI2 for ABA and salt stress (69) and phosphorylation of UBP24 by MPK3 might influence protein turnover of certain MAPK stress pathway components.

Besides identifying several direct known and novel MAPK substrates, our analysis also identified several indirect targets as downstream components of certain MAPKs. In addition to MAPKs, CDPKs represent an important protein kinase family involved in MAMP signaling. CPK4, CPK5, CPK6, and CPK11 were shown to be rapidly activated on flg22 treatment and are involved in the flg22-triggered oxidative burst and transcriptional reprogramming (51, 52). Several studies reported links between MAPKs and CDPKs, showing synergistic or antagonistic effects among these protein kinases (51, 75), but only a few CDPK substrates have been identified to date, including the plasma membrane-localized NADPH oxidase RBOHD as a substrate of CPK5 (60). Our phosphoproteomic analysis identified CPK5 and CPK6 to be phosphorylated indirectly via MPK3, MPK4, and MPK6. Interestingly, among the set of these indirect MAPK targets, we identified a number of proteins with a (K/R)xx(S/T)* phosphorylation consensus motif that could qualify as potential CDPK candidates. Among these, we find MAP65 with KVQEQPHVEQESAFSTRPSPARPV(s)*AKK, DRM1 (Dormancy-related protein 1) with the sequence KIT(t)*QPINIR or LSRPG(s)*GSVSGLASQR of PSD3 (phosphatidylserine decarboxylase 3). The involvement of immune MAPKs in the ROS burst production is still controversial. Several works suggest that the ROS burst is independent of MPK3/MPK6 or MPK4 (29, 76), whereas other works suggest that the ROS burst is at least partially dependent on MPK3/MPK6 or MPK4 (47, 77). In the case where immune MAPKs would contribute to the regulation of the MAMP-induced ROS burst, the *MAPK*-dependent regulation of CPK5 and CPK6 might constitute the underlying mechanism. Similarly, some of the acidophilic motifs detected in the genotype-dependent group could be the targets of casein kinases (CKs) (78). CK2 protein kinases are involved in multiple biological processes and in particular in immunity (79, 80). Our study might thus reveal new putative CDPK and CK targets that work in conjunction with MAPKs.

Our global phosphoproteomic analysis of WT plants and *mapk* mutants suggests the existence of a high intricacy between the immune-regulated MAPKs and their substrates. A selection of putative MAPK substrates was analyzed to assess the ability of immune MAPKs to both interact and phosphorylate these candidates. BiFC and pull-down data revealed interaction of these putative substrates with none up to the three MAPKs. BBC1 did not interact with any of the three MAPKs in these assays, and several candidate proteins were shown to interact with the MAPKs only in BiFC or pull-down assays. These could be false negative interactions that may arise for technical or biological reasons, for instance because the fusion of the candidate protein to a tag may result in aberrant protein folding or may sterically hinder the protein-protein interaction (81). Kinase assays followed by MS analysis confirmed the identification of the *in vivo* phosphosites and additional phosphorylated (S/T)*P sites were identified in some cases. The biological relevance of these new phosphosites would deserve being studied during normal development and in MAMP response. The phosphorylation of a given (S/T)*P site by a MAPK has been described to depend on several factors, among which are the presence and location of docking domains (82–84) and the kinase preference for the residues surrounding the phosphosite (72, 85). In line with this, our observations encourage considering a putative MAPK substrate at the level of each of its S*P or T*P phosphosites, anticipating that each site may be recognized and phosphorylated by a given MAPK with different affinities.

Novel MAPK Substrates—USPs belong to a superfamily and are found in bacteria, archaea, fungi, protozoa and plants. They are induced by various stresses to alter gene expression and resistance to stress (86, 87). Our work identified USPA to be phosphorylated at SPTVVTVQPS(s)*PRFPI(s)*TPTAGAQR in all *mapk* mutants *in vivo* on flg22 treatment. USPA interacted and was phosphorylated by all three MAPKs, suggesting that USPA is a shared *in vivo* substrate of MPK3, MPK4, and MPK6. The Arabidopsis USPs AtPHOS32 and AtPHOS34 are also phosphorylated on elicitation with *Phytophthora infestans*, xylanase and flg22, and AtPHOS32 S^{21} was identified as the flg22-triggered phosphosite (88, 89). *In vitro* kinase assays and immunodepletion assays indicated that MPK3 and MPK6 were the predominant protein kinases phosphorylating AtPHOS32 S^{21} residue (89). Overall, these combined data suggest that USPs might have an important role in plant defense downstream of the immune MAPKs.

Phosphorylation of BBC1 (an Arabidopsis ortholog of human Breast Basic Conserved protein 1) was reduced especially in *mpk6* (supplemental Fig. S2). *In vitro*, MPK4 and MPK6 could phosphorylate BBC1, making it a shared MAPK substrate.

TOM1 proteins in plants participate to the loading of the ESCRT (Endosomal Sorting Complex Required for Transport) machinery (90). We showed that TOM1 (AT5G16880) could interact with all three MAPKs and was phosphorylated *in vitro*

by MPK4 and MPK6. Because TOM1 showed significantly reduced phosphorylation in *mpk6* (supplemental Fig. S2), TOM1 appears to be mainly targeted by MPK6 *in vivo*. Another TOM1 (AT1G21380) showed absence of phosphorylation at (s)*PEHALFTKPVYDQTEQLPPAPWETQEPR in *mpk6*, suggesting that this protein is also an *in vivo* substrate of MPK6. These data would thus indicate that immune MAPKs, predominantly MPK6, regulate the ESCRT machinery.

Arabidopsis has 15 UBX (ubiquitin-regulatory X-containing) proteins that act as CDC48-interacting partners (91). PUX1 acts as a negative regulator of CDC48 regulating plant growth and development (92, 93). Interestingly, *pux2* showed reduced growth and reproduction of *Golovinomyces orontii* (91). We identified PUX9 to be phosphorylated in the three *mapk* mutants and in WT plants in response to flg22 treatment (supplemental Fig. S2). PUX9 interacted with and was phosphorylated by MPK3, MPK4 and MPK6, suggesting that PUX9 is a shared substrate of the three MAPKs *in vivo*.

UDP-glucose dehydrogenases (UGDs) belong to a four-membered family and provide cell wall precursors. A *ugd2ugd3* double mutant is compromised in primary cell wall formation (94), and infection of the double mutant by the cyst nematode *Heterodera schachtii* showed a severe defect in the development of feeding sites (95). We identified the phosphopeptide FDWDHPLHLQPM(s)*PTTVK whose sequence is shared by UGD2, UGD3, and UGD4. UGD2 interacted with and was phosphorylated by all three MAPKs. Interestingly, phosphorylation of FDWDHPLHLQPM(s)*PTTVK increased in *mpk4* but decreased in *mpk6* (supplemental Fig. S2), suggesting that the UGDs may be phosphorylated by the three MAPKs with variable affinities.

CaLB domain containing proteins affect the molecular interaction and subcellular localization of signaling proteins in a Ca^{2+}-dependent manner (96). The functions of CaLB domain proteins in plants are enigmatic, but one CaLB protein was shown to function as a transcriptional repressor of abiotic stress response (97). The sequence of CaLB LPLDID(s)*PTQSENSSSSQQ(t)*PK was phosphorylated on flg22 in WT but not in any of the three *mapk* mutants. We did not detect this phosphopeptide by *in vitro* kinase assays; yet we could detect the corresponding peptide in its nonphosphorylated version, which indicated that a lack of protein sequence coverage was not the issue. These results suggest that CaLB is probably not a direct substrate of MPK3, MPK4 or MPK6.

CONCLUSION

This work contributes to establishing a broader picture of MAPK substrates in plants. In agreement with their partially overlapping roles in plant defense, our results suggest that immune MAPKs have both specific and shared substrates, thereby contributing to the robustness of the defense signaling network. The intricate and exquisitely refined character of the immune MAPK substrate network likely expands to the other MAPKs. Our results also underline the fact that the entity to be defined as a specific or a shared substrate for MAPKs is not a phosphoprotein but a particular (S/T)P phosphorylation site in a given protein. This work also uncovers parts of the interplay between MAPKs and CDPKs. Finally, the proteins identified in this work constitute valuable candidates to better understand the exact roles of MAPKs and more generally the molecular mechanisms of signaling networks.

Acknowledgments—We would like to thank Véronique Legros and Huoming Zhang for technical assistance in MS, and Christophe Bruley, Véronique Dupierris and Emmanuelle Lastrucci (EDyP) for informatics support. We would like to thank Carlos Xavier Pita and Heno Hwang from KAUST for scientific Illustrations.

DATA AVAILABILITY

The mass spectrometry proteomics data have been deposited to the ProteomeXchange Consortium via the PRIDE partner repository with the dataset identifier PXD006807.

* This work was supported by the Agence Nationale de la Recherche (ANR-2010-JCJC-1608 to D. P.) and by the King Abdullah University of Science and Technology (BAS/1/1062–01-0). The IPS2 benefits from the support of the LabEx Saclay Plant Sciences-SPS (ANR-10-LABX-0040-SPS).

S This article contains supplemental material.

¶¶ To whom correspondence should be addressed: Center for Desert Agriculture, 4700 King Abdullah University of Science and Technology (KAUST), Thuwal, Saudi Arabia. Email: heribert.hirt@kaust.edu.sa.

|||| These authors contributed equally to this work.

Author Contributions: NR, JB, DP and HH designed the study. NR, JB, HA, JV and DP performed experimental work. NR, JB, LB, AH and DP performed *in silico* analysis and analyzed data. NR, JB, HA, DP and HH wrote the paper. All authors read and approved the manuscript.

REFERENCES

1. Bigeard, J., Rayapuram, N., Pflieger, D., and Hirt, H. (2014) Phosphorylation-dependent regulation of plant chromatin and chromatin-associated proteins. *Proteomics* **14,** 2127–2140
2. Rodriguez, M. C., Petersen, M., and Mundy, J. (2010) Mitogen-activated protein kinase signaling in plants. *Annu. Rev. Plant Biol.* **61,** 621–649
3. Beck, M., Komis, G., Muller, J., Menzel, D., and Samaj, J. (2010) Arabidopsis homologs of nucleus- and phragmoplast-localized kinase 2 and 3 and mitogen-activated protein kinase 4 are essential for microtubule organization. *Plant Cell* **22,** 755–771
4. Kosetsu, K., Matsunaga, S., Nakagami, H., Colcombet, J., Sasabe, M., Soyano, T., Takahashi, Y., Hirt, H., and Machida, Y. (2010) The MAP kinase MPK4 is required for cytokinesis in Arabidopsis thaliana. *Plant Cell* 22
5. Wang, H., Ngwenyama, N., Liu, Y., Walker, J. C., and Zhang, S. (2007) Stomatal development and patterning are regulated by environmentally responsive mitogen-activated protein kinases in Arabidopsis. *Plant Cell* **19,** 63–73
6. Jia, W., Li, B., Li, S., Liang, Y., Wu, X., Ma, M., Wang, J., Gao, J., Cai, Y., Zhang, Y., Wang, Y., Li, J., and Wang, Y. (2016) Mitogen-activated protein kinase cascade MKK7-MPK6 plays important roles in plant development and regulates shoot branching by phosphorylating PIN1 in Arabidopsis. *PLos Biol.* **14,** e1002550
7. Jones, J. D., and Dangl, J. L. (2006) The plant immune system. *Nature* **444,** 323–329
8. Bigeard, J., Colcombet, J., and Hirt, H. (2015) signaling mechanisms in pattern-triggered immunity (PTI). *Mol. Plant* **8,** 521–539

9. Gomez-Gomez, L., and Boller, T. (2000) FLS2: an LRR receptor-like kinase involved in the perception of the bacterial elicitor flagellin in Arabidopsis. *Mol. Cell* **5,** 1003–1011
10. Melotto, M., Underwood, W., and He, S. Y. (2008) Role of stomata in plant innate immunity and foliar bacterial diseases. *Annu. Rev. Phytopathol.* **46,** 101–122
11. Sawinski, K., Mersmann, S., Robatzek, S., and Bohmer, M. (2013) Guarding the green: pathways to stomatal immunity. *Mol. Plant Microbe Interact.* **26,** 626–632
12. Huckelhoven, R. (2007) Cell wall-associated mechanisms of disease resistance and susceptibility. *Annu. Rev. Phytopathol.* **45,** 101–127
13. Cowan, M. M. (1999) Plant products as antimicrobial agents. *Clin. Microbiol. Rev.* **12,** 564–582
14. van Loon, L. C., Rep, M., and Pieterse, C. M. (2006) Significance of inducible defense-related proteins in infected plants. *Annu. Rev. Phytopathol.* **44,** 135–162
15. Ahuja, I., Kissen, R., and Bones, A. M. (2012) Phytoalexins in defense against pathogens. *Trends Plant Sci.* **17,** 73–90
16. Bednarek, P. (2012) Chemical warfare or modulators of defence responses - the function of secondary metabolites in plant immunity. *Curr. Opin. Plant Biol.* **15,** 407–414
17. Asai, T., Tena, G., Plotnikova, J., Willmann, M. R., Chiu, W. L., Gomez-Gomez, L., Boller, T., Ausubel, F. M., and Sheen, J. (2002) MAP kinase signalling cascade in Arabidopsis innate immunity. *Nature* **415,** 977–983
18. Bethke, G., Pecher, P., Eschen-Lippold, L., Tsuda, K., Katagiri, F., Glazebrook, J., Scheel, D., and Lee, J. (2012) Activation of the Arabidopsis thaliana mitogen-activated protein kinase MPK11 by the flagellin-derived elicitor peptide, flg22. *Mol. Plant Microbe Interact.* **25,** 471–480
19. Eschen-Lippold, L., Bethke, G., Palm-Forster, M. A., Pecher, P., Bauer, N., Glazebrook, J., Scheel, D., and Lee, J. (2012) MPK11-a fourth elicitor-responsive mitogen-activated protein kinase in Arabidopsis thaliana. *Plant Signal Behav.* **7,** 1203–1205
20. Gao, M., Liu, J., Bi, D., Zhang, Z., Cheng, F., Chen, S., and Zhang, Y. (2008) MEKK1, MKK1/MKK2 and MPK4 function together in a mitogen-activated protein kinase cascade to regulate innate immunity in plants. *Cell Res.* **18,** 1190–1198
21. Nitta, Y., Ding, P., and Zhang, Y. (2014) Identification of additional MAP kinases activated on PAMP treatment. *Plant Signal Behav.* 9:e976155,
22. Ren, D., Yang, H., and Zhang, S. (2002) Cell death mediated by MAPK is associated with hydrogen peroxide production in Arabidopsis. *J. Biol. Chem.* **277,** 559–565
23. Qiu, J. L., Fiil, B. K., Petersen, K., Nielsen, H. B., Botanga, C. J., Thorgrimsen, S., Palma, K., Suarez-Rodriguez, M. C., Sandbech-Clausen, S., Lichota, J., Brodersen, P., Grasser, K. D., Mattsson, O., Glazebrook, J., Mundy, J., and Petersen, M. (2008) Arabidopsis MAP kinase 4 regulates gene expression through transcription factor release in the nucleus. *EMBO J.* **27,** 2214–2221
24. Pitzschke, A., Schikora, A., and Hirt, H. (2009) MAPK cascade signalling networks in plant defence. *Curr. Opin. Plant Biol.* **12,** 421–426
25. Ichimura, K., Casais, C., Peck, S. C., Shinozaki, K., and Shirasu, K. (2006) MEKK1 is required for MPK4 activation and regulates tissue-specific and temperature-dependent cell death in Arabidopsis. *J. Biol. Chem.* **281**
26. Petersen, M., Brodersen, P., Naested, H., Andreasson, E., Lindhart, U., Johansen, B., Nielsen, H. B., Lacy, M., Austin, M. J., Parker, J. E., Sharma, S. B., Klessig, D. F., Martienssen, R., Mattsson, O., Jensen, A. B., and Mundy, J. (2000) Arabidopsis map kinase 4 negatively regulates systemic acquired resistance. *Cell* **103,** 1111–1120
27. Suarez-Rodriguez, M. C., Adams-Phillips, L., Liu, Y., Wang, H., Su, S. H., Jester, P. J., Zhang, S., Bent, A. F., and Krysan, P. J. (2007) MEKK1 is required for flg22-induced MPK4 activation in Arabidopsis plants. *Plant Physiol.* **143**
28. Kong, Q., Qu, N., Gao, M., Zhang, Z., Ding, X., Yang, F., Li, Y., Dong, O. X., Chen, S., Li, X., and Zhang, Y. (2012) The MEKK1-MKK1/MKK2-MPK4 kinase cascade negatively regulates immunity mediated by a mitogen-activated protein kinase kinase kinase in Arabidopsis. *Plant Cell* **24,** 2225–2236
29. Zhang, Z., Wu, Y., Gao, M., Zhang, J., Kong, Q., Liu, Y., Ba, H., Zhou, J., and Zhang, Y. (2012) Disruption of PAMP-induced MAP kinase cascade by a Pseudomonas syringae effector activates plant immunity mediated by the NB-LRR protein SUMM2. *Cell Host Microbe* **11,** 253–263
30. Su, S. H., Bush, S. M., Zaman, N., Stecker, K., Sussman, M. R., and Krysan, P. (2013) Deletion of a tandem gene family in Arabidopsis: increased MEKK2 abundance triggers autoimmunity when the MEKK1-MKK1/2-MPK4 signaling cascade is disrupted. *Plant Cell* **25**
31. Frei dit Frey, N., Garcia, A. V., Bigeard, J., Zaag, R., Bueso, E., Garmier, M., Pateyron, S., de Tauzia-Moreau, M. L., Brunaud, V., Balzergue, S., Colcombet, J., Aubourg, S., Martin-Magniette, M. L., and Hirt, H. (2014) Functional analysis of Arabidopsis immune-related MAPKs uncovers a role for MPK3 as negative regulator of inducible defences. *Genome Biol.* **15,** R87
32. Hoehenwarter, W., Thomas, M., Nukarinen, E., Egelhofer, V., Rohrig, H., Weckwerth, W., Conrath, U., and Beckers, G. J. (2013) Identification of novel in vivo MAP kinase substrates in Arabidopsis thaliana through use of tandem metal oxide affinity chromatography. *Mol. Cell. Proteomics* **12,** 369–380
33. Lassowskat, I., Bottcher, C., Eschen-Lippold, L., Scheel, D., and Lee, J. (2014) Sustained mitogen-activated protein kinase activation reprograms defense metabolism and phosphoprotein profile in Arabidopsis thaliana. *Front. Plant Sci.* **5,** 554
34. Rayapuram, N., Bonhomme, L., Bigeard, J., Haddadou, K., Przybylski, C., Hirt, H., and Pflieger, D. (2014) Identification of novel PAMP-triggered phosphorylation and dephosphorylation events in Arabidopsis thaliana by quantitative phosphoproteomic analysis. *J. Proteome Res.* **13,** 2137–2151
35. Nakagami, H., Soukupova, H., Schikora, A., Zarsky, V., and Hirt, H. (2006) A Mitogen-activated protein kinase kinase kinase mediates reactive oxygen species homeostasis in Arabidopsis. *J. Biol. Chem.* **281,** 38697–38704
36. Mukhtar, M. S., Carvunis, A. R., Dreze, M., Epple, P., Steinbrenner, J., Moore, J., Tasan, M., Galli, M., Hao, T., Nishimura, M. T., Pevzner, S. J., Donovan, S. E., Ghamsari, L., Santhanam, B., Romero, V., Poulin, M. M., Gebreab, F., Gutierrez, B. J., Tam, S., Monachello, D., Boxem, M., Harbort, C. J., McDonald, N., Gai, L., Chen, H., He, Y., Vandenhaute, J., Roth, F. P., Hill, D. E., Ecker, J. R., Vidal, M., Beynon, J., Braun, P., and Dangl, J. L. (2011) Independently evolved virulence effectors converge onto hubs in a plant immune system network. *Science* **333,** 596–601
37. Vandenbogaert, M., Hourdel, V., Jardin-Mathe, O., Bigeard, J., Bonhomme, L., Legros, V., Hirt, H., Schwikowski, B., and Pflieger, D. (2012) Automated phosphopeptide identification using multiple MS/MS fragmentation modes. *J. Proteome Res.* **11,** 5695–5703
38. Savitski, M. M., Lemeer, S., Boesche, M., Lang, M., Mathieson, T., Bantscheff, M., and Kuster, B. (2011) Confident phosphorylation site localization using the Mascot Delta Score. *Mol. Cell. Proteomics* **10,** M110.003830
39. Cooper, H. J., Hakansson, K., Marshall, A. G., Hudgins, R. R., Haselmann, K. F., Kjeldsen, F., Budnik, B. A., Polfer, N. C., and Zubarev, R. A. (2003) Letter: the diagnostic value of amino acid side-chain losses in electron capture dissociation of polypeptides. Comment on: "Can the (M(.)-X) region in electron capture dissociation provide reliable information on amino acid composition of polypeptides?" *Eur. J. Mass Spectrom.* **8,** 461–469
40. Valot, B., Langella, O., Nano, E., and Zivy, M. (2011) MassChroQ: a versatile tool for mass spectrometry quantification. *Proteomics* **11,** 3572–3577
41. Cox, J., Hein, M. Y., Luber, C. A., Paron, I., Nagaraj, N., and Mann, M. (2014) Accurate proteome-wide label-free quantification by delayed normalization and maximal peptide ratio extraction, termed MaxLFQ. *Mol. Cell. Proteomics* **13,** 2513–2526
42. Schwartz, D., and Gygi, S. P. (2005) An iterative statistical approach to the identification of protein phosphorylation motifs from large-scale data sets. *Nat. Biotechnol.* **23,** 1391–1398
43. Franceschini, A., Szklarczyk, D., Frankild, S., Kuhn, M., Simonovic, M., Roth, A., Lin, J., Minguez, P., Bork, P., von Mering, C., and Jensen, L. J. (2013) STRING v9.1: protein-protein interaction networks, with increased coverage and integration. *Nucleic Acids Res.* **41,** D808–D815
44. Dinkel, H., Van Roey, K., Michael, S., Kumar, M., Uyar, B., Altenberg, B., Milchevskaya, V., Schneider, M., Kühn, H., Behrendt, A., Dahl, S. L., Damerell, V., Diebel, S., Kalman, S., Klein, S., Knudsen, A. C., Mäder, C., Merrill, S., Staudt, A., Thiel, V., Welti, L., Davey, N. E., Diella, F., and Gibson, T. J. (2016) ELM 2016—data update and new functionality of the eukaryotic linear motif resource. *Nucleic Acids Res.* **44,** D294–D300

45. Azimzadeh, J., Nacry, P., Christodoulidou, A., Drevensek, S., Camilleri, C., Amiour, N., Parcy, F., Pastuglia, M., and Bouchez, D. (2008) Arabidopsis TONNEAU1 proteins are essential for preprophase band formation and interact with centrin. *Plant Cell* **20,** 2146–2159
46. Nakagawa, T., Kurose, T., Hino, T., Tanaka, K., Kawamukai, M., Niwa, Y., Toyooka, K., Matsuoka, K., Jinbo, T., and Kimura, T. (2007) Development of series of gateway binary vectors, pGWBs, for realizing efficient construction of fusion genes for plant transformation. *J. Biosci. Bioeng.* **104,** 34–41
47. Berriri, S., Garcia, A. V., Frei dit Frey, N., Rozhon, W., Pateyron, S., Leonhardt, N., Montillet, J. L., Leung, J., Hirt, H., and Colcombet, J. (2012) Constitutively active mitogen-activated protein kinase versions reveal functions of Arabidopsis MPK4 in pathogen defense signaling. *Plant Cell* **24,** 4281–4293
48. Voinnet, O., Rivas, S., Mestre, P., and Baulcombe, D. (2003) An enhanced transient expression system in plants based on suppression of gene silencing by the p19 protein of tomato bushy stunt virus. *Plant J.* **33,** 949–956
49. Schwartz, D., Chou, M. F., and Church, G. M. (2009) Predicting protein post-translational modifications using meta-analysis of proteome scale data sets. *Mol. Cell. Proteomics* **8,** 365–379
50. Harper, J. F., and Harmon, A. (2005) Plants, symbiosis and parasites: a calcium signalling connection. *Nat. Rev. Mol. Cell Biol.* **6,** 555–566
51. Boudsocq, M., Willmann, M. R., McCormack, M., Lee, H., Shan, L., He, P., Bush, J., Cheng, S. H., and Sheen, J. (2010) Differential innate immune signalling via Ca(2+) sensor protein kinases. *Nature* **464,** 418–422
52. Romeis, T., and Herde, M. (2014) From local to global: CDPKs in systemic defense signaling upon microbial and herbivore attack. *Curr. Opin. Plant Biol.* **20,** 1–10
53. Wu, R., Dephoure, N., Haas, W., Huttlin, E. L., Zhai, B., Sowa, M. E., and Gygi, S. P. (2011) Correct interpretation of comprehensive phosphorylation dynamics requires normalization by protein expression changes. *Mol. Cell. Proteomics* **10,** M111.009654
54. Oliveira, A. P., Ludwig, C., Picotti, P., Kogadeeva, M., Aebersold, R., and Sauer, U. (2012) Regulation of yeast central metabolism by enzyme phosphorylation. *Mol. Syst. Biol.* **8,** 623
55. Zhang, H., Zhou, H., Berke, L., Heck, A. J., Mohammed, S., Scheres, B., and Menke, F. L. (2013) Quantitative phosphoproteomics after auxin-stimulated lateral root induction identifies an SNX1 protein phosphorylation site required for growth. *Mol. Cell. Proteomics* **2,** 1158–1169
56. MAPK-Group. (2002) Mitogen-activated protein kinase cascades in plants: a new nomenclature. *Trends Plant Sci.* **7,** 301–308
57. Hamada, T., Nagasaki-Takeuchi, N., Kato, T., Fujiwara, M., Sonobe, S., Fukao, Y., and Hashimoto, T. (2013) Purification and characterization of novel microtubule-associated proteins from Arabidopsis cell suspension cultures. *Plant Physiol.* **163,** 1804–1816
58. Abel, S., Bürstenbinder, K., and Müller, J. (2013) The emerging function of IQD proteins as scaffolds in cellular signaling and trafficking. *Plant Signal Behav.* **8,** e24369
59. Vos, J. W., Pieuchot, L., Evrard, J. L., Janski, N., Bergdoll, M., de Ronde, D., Perez, L. H., Sardon, T., Vernos, I., and Schmit, A. C. (2008) The plant TPX2 protein regulates prospindle assembly before nuclear envelope breakdown. *Plant Cell* **20,** 2783–2797
60. Dubiella, U., Seybold, H., Durian, G., Komander, E., Lassig, R., Witte, C. P., Schulze, W. X., and Romeis, T. (2013) Calcium-dependent protein kinase/NADPH oxidase activation circuit is required for rapid defense signal propagation. *Proc. Natl. Acad. Sci. U.S.A.* **110,** 8744–8749
61. Ling, Y., Alshareef, S., Butt, H., Lozano-Juste, J., Li, L., Galal, A. A., Moustafa, A., Momin, A. A., Tashkandi, M., Richardson, D. N., Fujii, H., Arold, S., Rodriguez, P. L., Duque, P., and Mahfouz, M. M. (2017) Pre-mRNA splicing repression triggers abiotic stress signaling in plants. *Plant J.* **89,** 291–309
62. de la Fuente van Bentem, S., Anrather, D., Dohnal, I., Roitinger, E., Csaszar, E., Joore, J., Buijnink, J., Carreri, A., Forzani, C., Lorkovic, Z. J., Barta, A., Lecourieux, D., Verhounig, A., Jonak, C., and Hirt, H. (2008) Site-specific phosphorylation profiling of Arabidopsis proteins by mass spectrometry and peptide chip analysis. *J. Proteome Res.* **7,** 2458–2470
63. Anderson, J. C., Bartels, S., Gonzalez Besteiro, M. A., Shahollari, B., Ulm, R., and Peck, S. C. (2011) Arabidopsis MAP Kinase Phosphatase 1 (AtMKP1) negatively regulates MPK6-mediated PAMP responses and resistance against bacteria. *Plant J.* **67,** 258–268
64. Bartels, S., Anderson, J. C., Gonzalez Besteiro, M. A., Carreri, A., Hirt, H., Buchala, A., Metraux, J. P., Peck, S. C., and Ulm, R. (2009) MAP kinase phosphatase1 and protein tyrosine phosphatase1 are repressors of salicylic acid synthesis and SNC1-mediated responses in Arabidopsis. *Plant Cell* **21,** 2884–2897
65. Park, H. C., Song, E. H., Nguyen, X. C., Lee, K., Kim, K. E., Kim, H. S., Lee, S. M., Kim, S. H., Bae, D. W., Yun, D. J., and Chung, W. S. (2011) Arabidopsis MAP kinase phosphatase 1 is phosphorylated and activated by its substrate AtMPK6. *Plant Cell Rep.* **30,** 1523–1531
66. Gonzalez Besteiro, M. A., and Ulm, R. (2013) Phosphorylation and stabilization of Arabidopsis MAP kinase phosphatase 1 in response to UV-B stress. *J. Biol. Chem.* **288,** 480–486
67. Janicka-Russak, M. (2011) *Plant Plasma Membrane H+-ATPase in Adaptation of Plants to Abiotic Stresses, Abiotic Stress Response in Plants*, INTECH
68. Liu, J., Elmore, J. M., Fuglsang, A. T., Palmgren, M. G., Staskawicz, B. J., and Coaker, G. (2009) RIN4 functions with plasma membrane H+-ATPases to regulate stomatal apertures during pathogen attack. *PLos Biol.* **7,** e1000139
69. Zhao, J., Zhou, H., Zhang, M., Gao, Y., Li, L., Gao, Y., Li, M., Yang, Y., Guo, Y., and Li, X. (2016) Ubiquitin-specific protease 24 negatively regulates abscisic acid signalling in Arabidopsis thaliana. *Plant Cell Environ.* **39,** 427–440
70. Danquah, A., de Zelicourt, A., Boudsocq, M., Neubauer, J., Frei Dit Frey, N., Leonhardt, N., Pateyron, S., Gwinner, F., Tamby, J. P., Ortiz-Masia, D., Marcote, M. J., Hirt, H., and Colcombet, J. (2015) Identification and characterization of an ABA-activated MAP kinase cascade in Arabidopsis thaliana. *Plant J.* **82,** 232–244
71. Popescu, S. C., Popescu, G. V., Bachan, S., Zhang, Z., Gerstein, M., Snyder, M., and Dinesh-Kumar, S. P. (2009) MAPK target networks in Arabidopsis thaliana revealed using functional protein microarrays. *Genes Dev.* **23,** 80–92
72. Sorensson, C., Lenman, M., Veide-Vilg, J., Schopper, S., Ljungdahl, T., Grotli, M., Tamas, M. J., Peck, S. C., and Andreasson, E. (2012) Determination of primary sequence specificity of Arabidopsis MAPKs MPK3 and MPK6 leads to identification of new substrates. *Biochem. J.* **446,** 271–278
73. Feilner, T., Hultschig, C., Lee, J., Meyer, S., Immink, R. G., Koenig, A., Possling, A., Seitz, H., Beveridge, A., Scheel, D., Cahill, D. J., Lehrach, H., Kreutzberger, J., and Kersten, B. (2005) High throughput identification of potential Arabidopsis mitogen-activated protein kinases substrates. *Mol. Cell. Proteomics* **4,** 1558–1568
74. Courcelles, M., Fremin, C., Voisin, L., Lemieux, S., Meloche, S., and Thibault, P. (2013) Phosphoproteome dynamics reveal novel ERK1/2 MAP kinase substrates with broad spectrum of functions. *Mol. Syst. Biol.* **9,** 669
75. Ludwig, A. A., Saitoh, H., Felix, G., Freymark, G., Miersch, O., Wasternack, C., Boller, T., Jones, J. D., and Romeis, T. (2005) Ethylene-mediated cross-talk between calcium-dependent protein kinase and MAPK signaling controls stress responses in plants. *Proc. Natl. Acad. Sci. U.S.A.* **102,** 10736–10741
76. Xu, J., Xie, J., Yan, C., Zou, X., Ren, D., and Zhang, S. (2014) A chemical genetic approach demonstrates that MPK3/MPK6 activation and NADPH oxidase-mediated oxidative burst are two independent signaling events in plant immunity. *Plant J.* **77,** 222–234
77. Ranf, S., Eschen-Lippold, L., Pecher, P., Lee, J., and Scheel, D. (2011) Interplay between calcium signalling and early signalling elements during defence responses to microbe- or damage-associated molecular patterns. *Plant J.* **68,** 100–113
78. Meggio, F., Perich, J. W., Reynolds, E. C., and Pinna, L. A. (1991) A synthetic beta-casein phosphopeptide and analogues as model substrates for casein kinase-1, a ubiquitous, phosphate directed protein kinase. *FEBS Lett.* **283,** 303–306
79. Hidalgo, P., Garreton, V., Berrios, C. G., Ojeda, H., Jordana, X., and Holuigue, L. (2001) A nuclear casein kinase 2 activity is involved in early events of transcriptional activation induced by salicylic acid in tobacco. *Plant Physiol.* **125,** 396–405
80. Kang, H. G., and Klessig, D. F. (2005) Salicylic acid-inducible Arabidopsis CK2-like activity phosphorylates TGA2. *Plant Mol. Biol.* **57,** 541–557
81. Kudla, J., and Bock, R. (2016) Lighting the way to protein-protein interactions: recommendations on best practices for bimolecular fluorescence complementation analyses. *Plant Cell* **28,** 1002–1008

82. Jacobs, D., Glossip, D., Xing, H., Muslin, A. J., and Kornfeld, K. (1999) Multiple docking sites on substrate proteins form a modular system that mediates recognition by ERK MAP kinase. *Genes Dev.* **13,** 163–175
83. Biondi, R. M., and Nebreda, A. R. (2003) Signalling specificity of Ser/Thr protein kinases through docking-site-mediated interactions. *Biochem. J.* **372,** 1–13
84. Sheridan, D. L., Kong, Y., Parker, S. A., Dalby, K. N., and Turk, B. E. (2008) Substrate discrimination among mitogen-activated protein kinases through distinct docking sequence motifs. *J. Biol. Chem.* **283,** 19511–19520
85. Berriri, S., Garcia, A. V., Dit Frey, N. F., Rozhon, W., Pateyron, S., Leonhardt, N., Montillet, J. L., Leung, J., Hirt, H., and Colcombet, J. (2012) Constitutively active mitogen-activated protein kinase versions reveal functions of Arabidopsis MPK4 in pathogen defense signaling. *Plant Cell* **24**
86. Siegele, D. A. (2005) Universal stress proteins in Escherichia coli. *J. Bacteriol.* **187,** 6253–6254
87. Tkaczuk, K. L., I, A. S., Chruszcz, M., Evdokimova, E., Savchenko, A., and Minor, W. (2013) Structural and functional insight into the universal stress protein family. *Evol. Appl.* **6,** 434–449
88. Lenman, M., Sorensson, C., and Andreasson, E. (2008) Enrichment of phosphoproteins and phosphopeptide derivatization identify universal stress proteins in elicitor-treated Arabidopsis. *Mol. Plant Microbe Interact.* **21,** 1275–1284
89. Merkouropoulos, G., Andreasson, E., Hess, D., Boller, T., and Peck, S. C. (2008) An Arabidopsis protein phosphorylated in response to microbial elicitation, AtPHOS32, is a substrate of MAP kinases 3 and 6. *J. Biol. Chem.* **283,** 10493–10499
90. Winter, V., and Hauser, M. T. (2006) Exploring the ESCRTing machinery in eukaryotes. *Trends Plant Sci.* **11,** 115–123
91. Chandran, D., Tai, Y. C., Hather, G., Dewdney, J., Denoux, C., Burgess, D. G., Ausubel, F. M., Speed, T. P., and Wildermuth, M. C. (2009) Temporal global expression data reveal known and novel salicylate-impacted processes and regulators mediating powdery mildew growth and reproduction on Arabidopsis. *Plant Physiol.* **149,** 1435–1451
92. Park, S., Rancour, D. M., and Bednarek, S. Y. (2007) Protein domain-domain interactions and requirements for the negative regulation of Arabidopsis CDC48/p97 by the plant ubiquitin regulatory X (UBX) domain-containing protein, PUX1. *J. Biol. Chem.* **282,** 5217–5224
93. Rancour, D. M., Park, S., Knight, S. D., and Bednarek, S. Y. (2004) Plant UBX domain-containing protein 1, PUX1, regulates the oligomeric structure and activity of arabidopsis CDC48. *J. Biol. Chem.* **279,** 54264–54274
94. Reboul, R., Geserick, C., Pabst, M., Frey, B., Wittmann, D., Lutz-Meindl, U., Leonard, R., and Tenhaken, R. (2011) Down-regulation of UDP-glucuronic acid biosynthesis leads to swollen plant cell walls and severe developmental defects associated with changes in pectic polysaccharides. *J. Biol. Chem.* **286,** 39982–39992
95. Siddique, S., Sobczak, M., Tenhaken, R., Grundler, F. M., and Bohlmann, H. (2012) Cell wall ingrowths in nematode induced syncytia require UGD2 and UGD3. *PLoS ONE* **7,** e41515
96. Gawler, D. J., Zhang, L. J., Reedijk, M., Tung, P. S., and Moran, M. F. (1995) CaLB: a 43 amino acid calcium-dependent membrane/phospholipid binding domain in p120 Ras GTPase-activating protein. *Oncogene* **10,** 817–825
97. de Silva, K., Laska, B., Brown, C., Sederoff, H. W., and Khodakovskaya, M. (2011) Arabidopsis thaliana calcium-dependent lipid-binding protein (AtCLB): a novel repressor of abiotic stress response. *J. Exp. Bot.* **62,** 2679–2689
98. Wroblewski, T., Caldwell, K. S., Piskurewicz, U., Cavanaugh, K. A., Xu, H., Kozik, A., Ochoa, O., McHale, L. K., Lahre, K., Jelenska, J., Castillo, J. A., Blumenthal, D., Vinatzer, B. A., Greenberg, J. T., and Michelmore, R. W. (2009) Comparative large-scale analysis of interactions between several crop species and the effector repertoires from multiple pathovars of Pseudomonas and Ralstonia. *Plant Physiol.* **150,** 1733–1749